Tectonophysics 747–748 (2018) 357–372

Contents lists available at ScienceDirect

Tectonophysics

journal homepage: www.elsevier.com/locate/tecto

Earthquake environmental effects produced by the Mw 6.1, 20th May 2016 Petermann earthquake, Australia☆

King Tamarah R.[a,*], Quigley Mark C.[a], Clark Dan[b]

[a] School of Earth Sciences, University of Melbourne, Cnr Swanston and Elgin St., Carlton VIC 3053, Australia
[b] Geoscience Australia, Cnr Jerrabomberra Ave and Hindmarsh Drive, Symonston ACT 2609, Australia

ARTICLE INFO

Keywords:
ESI-07 scale
Earthquake Environmental Effects
Surface rupture
Intraplate earthquake
Australian earthquake

ABSTRACT

Earthquake Environmental Effects (EEEs) identified in the source region of the 20th May 2016 intraplate moment magnitude (M_w) 6.1 Petermann earthquake in Central Australia are described and classified using the Environmental Seismic Intensity (ESI-07) scale. EEEs include surface rupture, ground fissures and cracks, vegetation damage, rockfalls, and displaced (jumped) bedrock fragments. The maximum ESI intensity derived from EEEs is *X*, consistent with previous observations from some moderate M_w crustal earthquakes. Maximum ESI isoseismals correlate with the location of the surface rupture rather than epicentre area due to the dipping geometry of the reverse source fault. ESI isoseismals encompass a larger area of the hanging-wall than the footwall, indicating stronger ground motions on the hanging-wall due to increased proximity to the rupture source and ground motion amplification effects. The maximum areal extent of secondary (seismic shaking-induced) EEEs (300 km^2) is significantly smaller than expected using the published ESI-07 scale (approx. 5000 km^2). This relates to the low topographic relief and relatively homogeneous bedrock geology of the study region, which (i) reduced the potential for site response amplification of strong ground motions, and *(ii)* reduced the susceptibility of the landscape to EEE such as landsliding and liquefaction. Erosional degradation of the observed EEE features and decreasing confidence with which they can be uniquely attributed to a seismic origin with increasing time since the earthquake highlight challenges in using many of the natural features observed herein to characterise the locations and attributes of paleo-earthquakes.

1. Background

1.1. Introduction

Earthquake Environmental Effects (EEEs) are the observable physical changes and damage resulting from moderate to large earthquakes on local geology, geomorphology, hydrology, botany and topography (Guerrieri et al., 2007). The 2007 Environmental Seismic Intensity (ESI-07) scale provides a standardized method of quantifying the size of various EEEs with relation to earthquake intensity (Guerrieri et al., 2007; Michetti et al., 2007). It has most commonly been applied to estimate the intensity of recent earthquakes (Ali et al., 2009; Ota et al., 2009; Papanikolaou and Melaki, 2017; Papanikolaou et al., 2009; Papathanassiou et al., 2017; Rodríguez-Pascua et al., 2017; Sanchez and Maldonado, 2016) and historic earthquakes (Papanikolaou and Melaki, 2017; Silva et al., 2009). The ESI-07 scale was partly developed as a tool for palaeoseismic investigation to enable comparison of recent, historic and pre-historic earthquakes by investigating and documenting EEEs.

As discussed in Serva et al. (2016) and Quigley et al. (2016), EEEs may vary significantly in the prominence of their expression due to aspects of the seismic source (e.g., magnitude, rupture kinematics, directivity effects) and site conditions (e.g., geologic heterogeneity, basin effects, topographic effects). This may alter EEE inducing ground motions and the vulnerability of a given feature to recording EEEs under imposed seismic shaking. Documentation of EEEs in diverse tectonic and geomorphic environments is important to improve the confidence in using EEEs to characterise seismic source attributes and estimate ESI metrics (Blumetti et al., 2017).

The 20th May (UTC) 2016 M_w 6.1 Petermann earthquake in central Australia was a moderate magnitude intraplate earthquake with a well-constrained location, depth, mechanism, magnitude and geometrically simple rupture (Fig. 1). The epicentral region is characterised by low rainfall, subdued relief, extremely low bedrock erosion rates (Bierman

☆ No declarations of interest.

* Corresponding author.
E-mail addresses: tamarah.king@unimelb.edu.au (T.R. King), mark.quigley@unimelb.edu.au (M.C. Quigley), dan.clark@ga.gov.au (D. Clark).

https://doi.org/10.1016/j.tecto.2018.10.010
Received 5 July 2018; Received in revised form 4 October 2018; Accepted 6 October 2018
Available online 14 October 2018

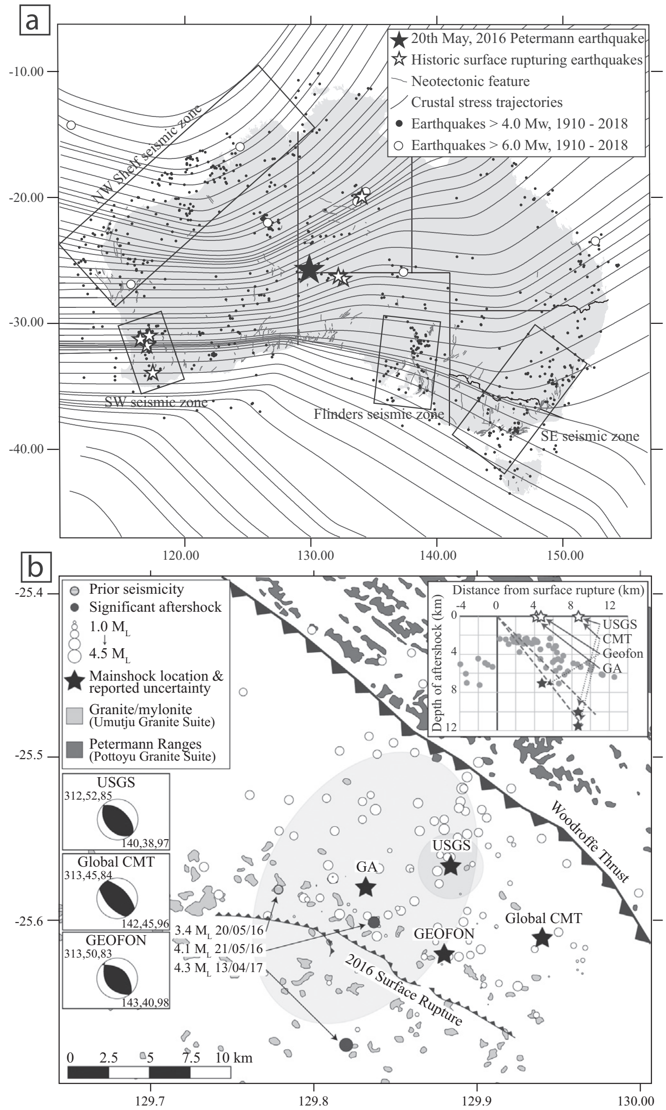

Fig. 1. Seismotectonic maps of (a) regional historic seismicity (Geoscience Australia catalogue, https://earthquakes.ga.gov.au/), historic surface rupturing earthquakes (Clark et al., 2014), seismic zones (Leonard, 2008), neotectonic faults (Clark et al., 2012) and crustal stress orientations (Rajabi et al., 2017) (b) seismology and geology of the Petermann earthquake including published focal mechanisms, available instrumental epicentres and aleatoric uncertainties, available hypocentre depths, major geological features and available aftershock locations and depths (GG-Cat, 30/10/17).

and Caffee, 2002), sparse vegetation, and has been subject to minimal changes in climate since the end of the last glacial (Chen et al., 1993; Hesse, 2010). A range of primary and secondary EEEs were observed following the main shock, including surface rupture, rock falls, ground cracking, displaced rocks and vegetation damage. We have categorised and classified 3967 EEEs using the ESI-07 scale. The location of the earthquake in a remote, geologically homogenous region of subdued relief allows for observation of EEEs and interpretation of ESI intensity patterns, largely free from site-effects (e.g. topography, geology, basin effects, regolith thickness changes, built environment effects). The event therefore provides a rare opportunity to investigate the relationship between EEEs and the seismic source (epicentre, fault rupture location, geometry, and kinematics) without common complicating factors that influence many other settings on earth. Further, EEEs are unlikely to be destroyed by human activity, allowing for rates of natural degradation of the EEE ‘signal’ to be estimated.

Our findings show that EEEs correlate with the geometry of the rupture source (rather than the earthquake epicentre) and are strongly influenced by hanging-wall vs. footwall effects. Repeated observations of EEEs has allowed for estimates of palaeoseismic preservation in this slow changing environment, with implications for EEE preservation in more geomorphically active regions.

1.2. Seismotectonic setting

Australia is a stable continental region within the Indo-Australian plate, with distant active plate boundaries. The most recently published Australian stress map (Rajabi et al., 2017) demonstrates a variably orientated crustal stress field (Fig. 1a) aligned with convergent Indo-Australian plate boundaries. Australia experiences a > M_w 6.0 earthquake every 8 years on average (Leonard, 2008) with 12 recorded events since 1910 (Fig. 1a). Half of these have occurred in the cratonic continental interior, remote from previously recognised zones of high seismic activity (Leonard, 2008) (Fig. 1a). There have been eight documented historic surface rupturing events (Fig. 1a), ranging from the 1.6 km long 2012 M_w 5.4 Pukatja (Ernabella) earthquake (Clark et al., 2014), to the 37 km long 1968 M_w 6.8 Meckering earthquake (Gordon and Lewis, 1980). Historic surface ruptures have commonly been complex multi-fault ruptures comprising dominantly reverse and minor strike-slip movements depending upon the azimuthal angle between the fault orientation and the prevailing maximum horizontal present-day stress field (Clark and McCue, 2003).

Detailed palaeoseismic investigations in Australia have focused on areas that correspond with topographic anomalies and higher historic seismicity, as well as being in regions that are relatively easy to access for trenching and field investigations (Clark et al., 2011; Quigley et al., 2010). Neotectonic structures and folds have been identified based on clear structural evidence, traditional geomorphic markers such as offset geomorphology/waterways and young talus slopes (Clark et al., 2008; Crone et al., 2003; Quigley et al., 2006), offset and warping within Miocene and younger sedimentary packages (Holdgate et al., 2008, 2003; Mcpherson et al., 2014; Wallace et al., 2005), and anomalous weathering rates across topographic features (Quigley et al., 2007b, 2007a). Several hundred potential surface rupturing neotectonic faults have been identified in SRTM digital elevation models and other data (Clark, 2010; Clark et al., 2011). These are freely available from Geoscience Australia's neotectonic features database (http://www.ga.gov.au/earthquakes/staticPageController.do?page=neotectonics) (Fig. 1a). Most have not been investigated in detail, due to remoteness and/or the low societal perception of earthquake risk in intraplate regions.

Despite the large number of neotectonic structures identified, all historic surface rupturing earthquakes have occurred on previously unknown cratonic faults with little to no prior geomorphic or topographic expression. These events highlight the difficulty in identifying active faults in intraplate settings using traditional palaeoseismic methods. EEEs potentially provide an additional investigative tool.

1.3. Seismology

The Petermann earthquake occurred near the Petermann Ranges of far south-west Northern Territory. Ground movements woke residents 115 km away in Yulara (Uluru) and in remote indigenous communities up to 250 km away. The United States Geological Survey (USGS) reported M_w 6.0 and depth of 10 km (± 1.7 km), while Geoscience Australia (GA) reported M_w 6.1 with no depth estimate (Fig. 1b). The closest seismometers were located 166 km west in Warakurna, Western Australia, and 505 km north-east in Alice Springs, Northern Territory. Reported epicentral uncertainties are shown on Fig. 1b.

High resolution aftershock data recorded on a temporary seismometer network are shown on Fig. 1b, obtained from GG-Cat (Allen et al., 2012) accessed on the 30th October 2017. During the 15 months that the temporary seismometer network was deployed and active, two > M_L 4.0 aftershocks including a M_L 4.3 on 13th April 2017 (11 months after the mainshock) were recorded (Fig. 1b). The only recorded earthquake in the area prior to the 20th May 2016 mainshock was a M_L 3.5 event on the 19th May 2016 (2 days before the mainshock) ~10 km from the mainshock location (Fig. 1b).

Available published moment tensors are included in Fig. 1b. The Petermann earthquake surface rupture has an average strike of ~294° and dips to the north-east (Fig. 1b). Sixty-five well located aftershocks with median aleatoric depth uncertainty of ± 0.23 km are plotted in Fig. 1b alongside the USGS preferred nodal plane solution of 52°, and Global CMT solution of 45°.The strike of the fault is orientated roughly perpendicular to calculated crustal stress trajectories for the region (Rajabi et al., 2017).

1.4. Geology

The 20th May 2016 Petermann earthquake occurred in the western Musgrave Block, a Mesoproterozoic basement province that stretches across the Northern Territory/South Australia border and into Western Australia, which formed predominately in the 580–520 Ma Petermann Orogeny (Edgoose et al., 2004). Two large structures, the Woodroffe Thrust and Mann Fault, dominated uplift and deformation during the Petermann Orogeny, displacing mid to lower-crustal metamorphic units which now form the Petermann and Mann Ranges. The 2016 Petermann earthquake ruptured through north-east dipping mylonite in the hanging-wall of the south west dipping Woodroffe Thrust. The surface trace of the Woodroffe Thrust is mapped ~10 km north-east of the 2016 rupture (Fig. 1b).

1.5. Geography

The Petermann earthquake occurred in vegetated desert punctuated by southeast-trending mid- to late Pleistocene longitudinal dunes (Hesse, 2010) up to several tens of kilometres long and 2–10 m in height. Sand dunes are well vegetated with spinifex (*Triodia*) and mature desert oak trees (A*llocasuarina decaisneana*) up to 10 m high with a canopy diameter up to 20 m. Adjacent low-lying land is vegetated with spinifex, groves of mulga bush (*Acacia aneura*) and sporadic desert oak trees (Robinson et al., 2003).

Isolated granite and gneiss hills rise prominently up to 100 m above the desert surface while outcrops of mylonite occur locally in inter-dune regions, generally outcropping as multiple outcrops each 1–10 m in diameter and < 5 m high (Fig. 1b and Fig. 2). Sediments overlying bedrock are typically skeletal and related to sheet-wash and aeolian processes, except where Tertiary paleo-valley systems contain several tens of metres of fluvial, lacustrine and chemical sediments (Bell et al., 2012).

The area experienced abnormally high rainfall in the year following the 20th May 2016 earthquake with record high rainfall recorded by the Bureau of Meteorology (bom.gov.au) for June 2016 (at Giles Meteorological Office, 172 km north-west), August 2016 (at Yulara Airport, 116 km north-east), and December 2016 (at Curtin Springs, 190 km east). The months of May 2016, June 2016, December 2016 and January 2017 also saw the second highest monthly rainfall recorded at Yulara since records began in 1983. In the immediate vicinity of the fault, drainage from infrequent rains occurs in small inter-dune playas, palaeovalleys and vehicle tracks.

2. Observed environmental effects

2.1. Data collection and field seasons

The epicentral area was accessed via an unsealed access track (Fig. 2) approximately 150 km from the town of Yulara (Uluru). A prompt field response was arranged to investigate the epicentral region for a surface rupture and environmental damage, with a second season completed 16 months after the event. All EEE data collected in this time is shown in Fig. 2. Fig. 3 summarises the field response including the duration of fieldwork, available data at the time of field work, equipment used, and data collected. This summary demonstrates the progressive nature of data collection during an earthquake response, and some of the complicating factors inhibiting data collection.

Field teams responded with temporary seismometers within 3 days of the event but ground observations of the surface rupture were first made 20 days after the earthquake due to rainfall that inhibited field work. Giles meteorological station recorded 85.5 mm of rain falling during that time (~30% of annual mean rainfall). Travel to and along the region of maximum surface offset was limited to foot traverses.

2.2. Surface rupture

Surface rupturing during the 2016 event occurred in segments along a ~20 km arcuate NW-SE trending trace (Fig. 2). Some sections of the 2016 rupture warped the surface sediments rather than resulting in discrete surface rupture. For the purposes of this paper discrete rupture refers to clear dislocation of the hanging-wall and footwall along the fault plane, while warping or folding refer to areas of hanging-wall vertical uplift relative to the footwall along strike of the rupture, but with no visible dislocation. The varieties of rupture types and their interaction with surface cover and bedrock are illustrated in Fig. 4.

Evidence for discrete rupture or warping along the rupture trace was discontinuous (Fig. 2), particularly towards the NW and SE tips of rupture and where passing through dunes. The geometry of the rupture suggests the earthquake ruptured two segments, transferring from a NW - SE structure in the southeast, to a more E-W structure to the northwest, creating a convex shape, with a large step-over ~8 km from its north-western most tip (Fig. 2). Vertical offset along ruptured sections varied from < 0.05 m up to a maximum of 0.9 m (Fig. 2).

The magnitude of vertical offset and strike direction of the scarp varied over short distances, typically corresponding with dune topographic or lithological changes (Fig. 4). Vertical offset maximums generally occurred in semi-consolidated sandy environments with bedrock or calcrete at or near the surface (Fig. 4a, b). In some areas broad warping is visible with no discrete rupture of surface sediment (Fig. 4c, d). In two locations on dune slopes where loose calcrete clasts dominate the surface and subsurface, rupture consisted of discontinuous topographic bulges (mole tracks) and extensional cracks (Fig. 4e, f). Hanging-wall sediments are thrust over bedrock outcrop in at least two locations (Fig. 4i). In one instance, hanging-wall sediments are thrust against a ~1 m high mylonite outcrop with a strike and dip that matches the 2016 rupture (Fig. 4j).

Fault tip folding occurred on the hanging-wall within 5 m of discrete rupture along certain sections (Fig. 4g, h). Rupture parallel extensional cracking is associated with this folding. Sections where discrete rupture and hanging-wall folding occurred generally ruptured through flat intra-dune areas with more consolidated sheet-wash and aeolian sand/dust surface cover and near-surface calcrete or bedrock. These long sections of surface rupture often contain back-steps in rupture and multiple duplexing discrete ruptures (Fig. 4h).

2.3. Cracking

Coseismic extensional (Fig. 5a,b), transtensional (Fig. 5c,d), compressional (Fig. 5e,f) and mole track (Fig. 5e) cracking was observed along all mapped segments of the surface rupture, and within 7 km from the surface rupture on the hanging-wall. Field observations were obtained primarily along the trace of the surface rupture, on fault perpendicular traverses, and on large outcrops at distances of 2–50 km from the scarp (Fig. 2). Cracks documented on traverses were only those large enough to be easily observed between ground covering vegetation while walking. The dataset is therefore incomplete spatially and in crack size across the area.

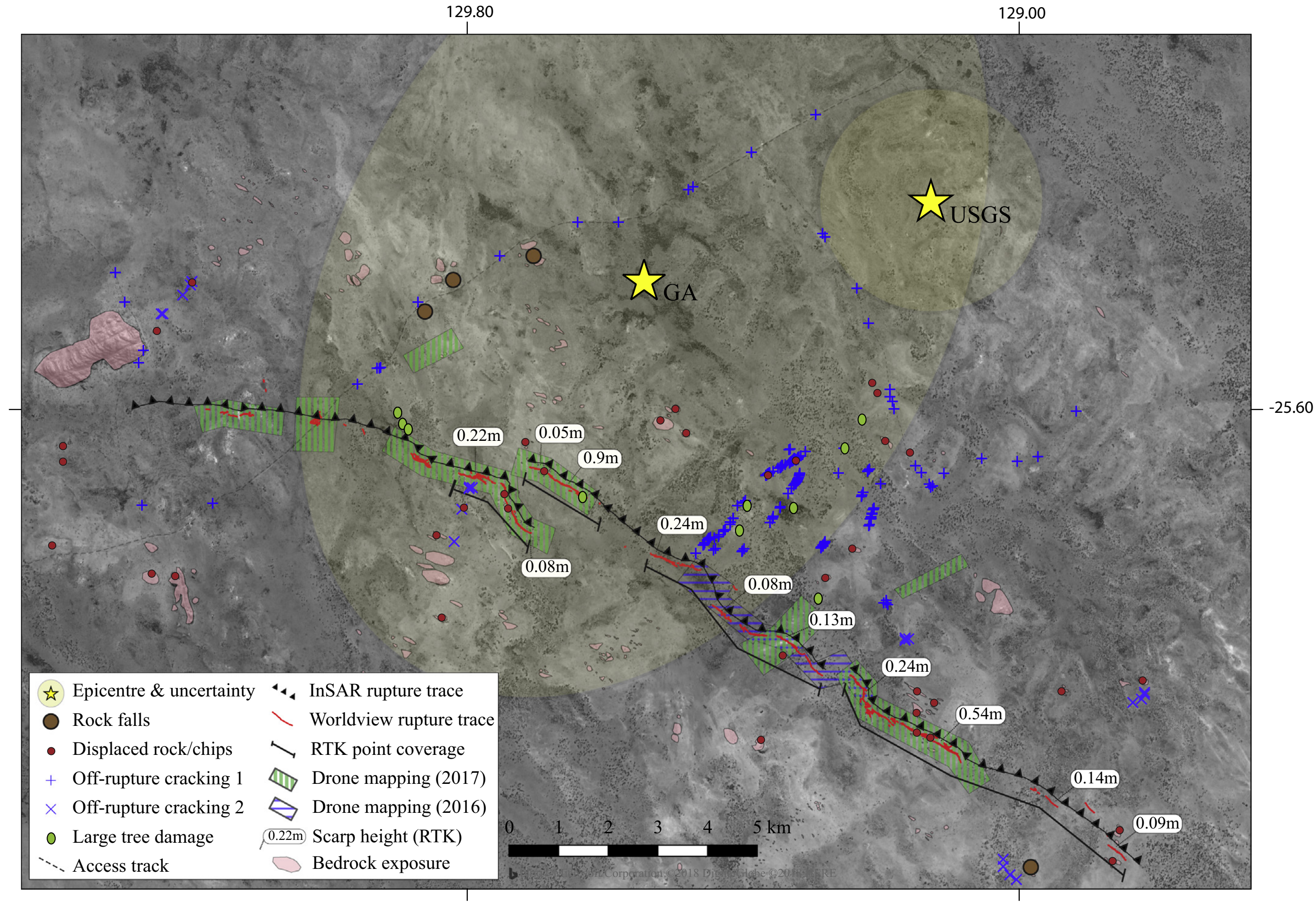

Fig. 2. Distribution of observed EEEs including extent of surface rupture deformation as observed on InSAR and discrete surface rupture as observed in the field and satellite imagery. Drone imagery overlap from 2016 and 2017 provides comparison for denudation of EEEs. Off-rupture cracking 2 are data observed 16 months after the mainshock, and potentially related to aftershocks.

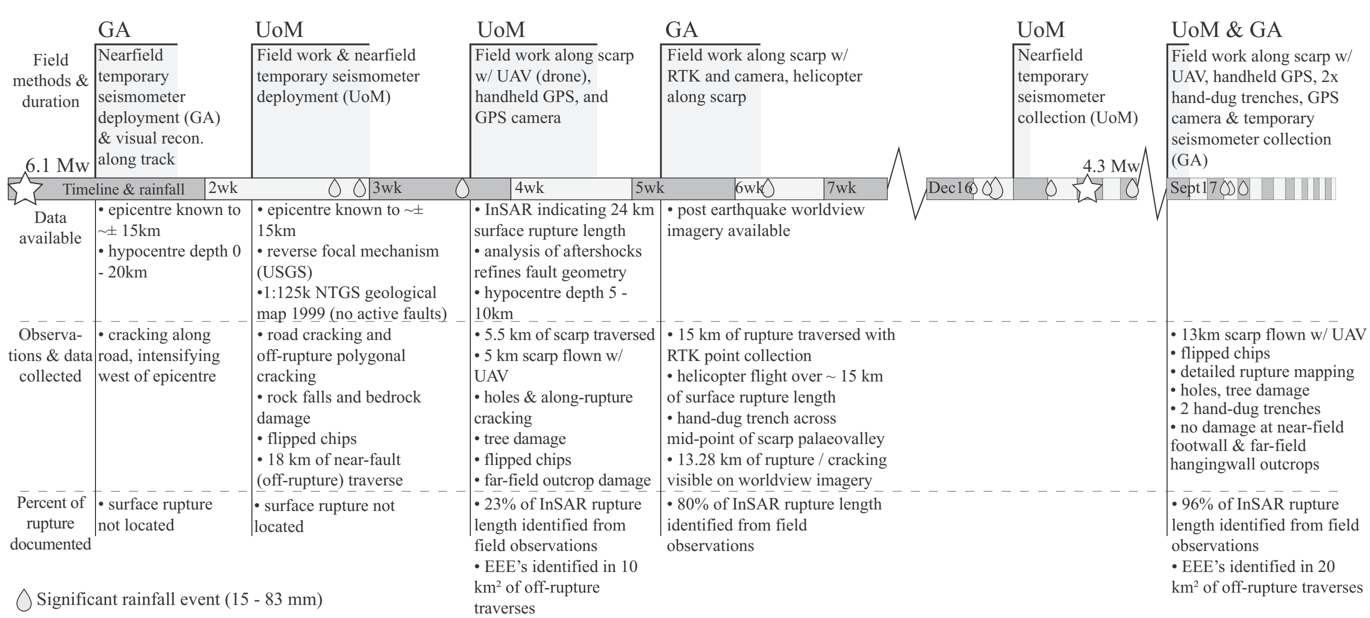

Fig. 3. Timeline of field-work methods and observations following the 20th May 2016 Petermann earthquake. Timeline demonstrates the progressive nature of data collection during a remote earthquake response and complicating factors such as data-set availability and significant weather events.

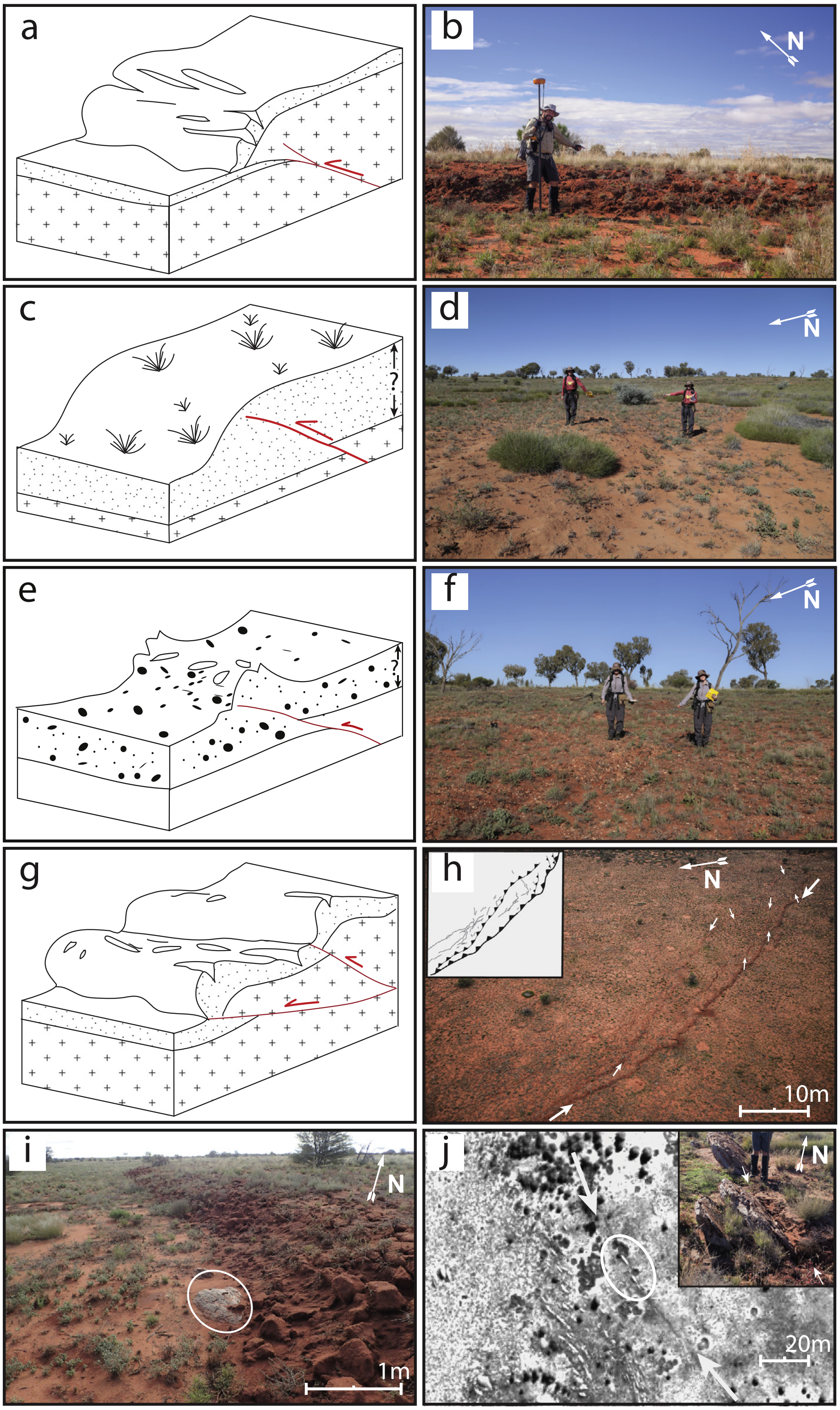

Fig. 4. Rupture styles observed along the Petermann scarp including (a) discrete surface rupture with fault parallel folding and cracking, near surface bedrock or calcrete and sediment collapse along the rupture front (b) image of discrete surface rupture in region of maximum vertical offset (c) broad warping in sandy sediment with unknown depth to bedrock/calcrete and no discrete rupture front (d) composite image of author on either side of broad warping (e) mole tracks where loose calcrete clasts dominate surface sediments, with unknown depth to in-situ bedrock/calcrete and extensional cracking along topographic bulges (f) composite image of author on either side of mole tracks (g) duplexing discrete ruptures and fault tip folding in areas with shallow bedrock/calcrete (h) helicopter image of duplexing discrete ruptures including schematic map of image (i) bedrock in the foot-wall along rupture zone with maximum vertical offset (j) hanging-wall sediment thrust against bedrock outcrop with the same dip and strike as the rupture, white arrows highlight rupture.

Edge collapse of extensional cracks due to rainfall and slope instability made these cracks the most obvious, and therefore the most commonly documented. Compressional cracking (i.e. pop-ups and mole-tracks) were less visible between the abundant low-growing spinifex and grasses and easily destroyed by rainfall runoff and animal movement (camels, kangaroos, dingos and various small marsupials). Most observed cracks occurred between dunes in silty and/or clay-rich sands, clay-pans and playas, though some were also observed at the apex of well vegetated and stable dunes included during the second field season over a year later.

Cracks along vehicular tracks often occurred on the soft sediment piled up to the verges from annual maintenance (Fig. 5h). These occurred parallel to the tracks which were commonly perpendicular to the surface rupture, suggesting a rheological control (i.e. between the firm track and the soft side sediment).

Extensional cracks are distributed across the field area, with lengths commonly < 2 m and widths between 0.5 and 5 cm. The two largest cracks are 80 m long with up to 24 cm extension at the surface (due in

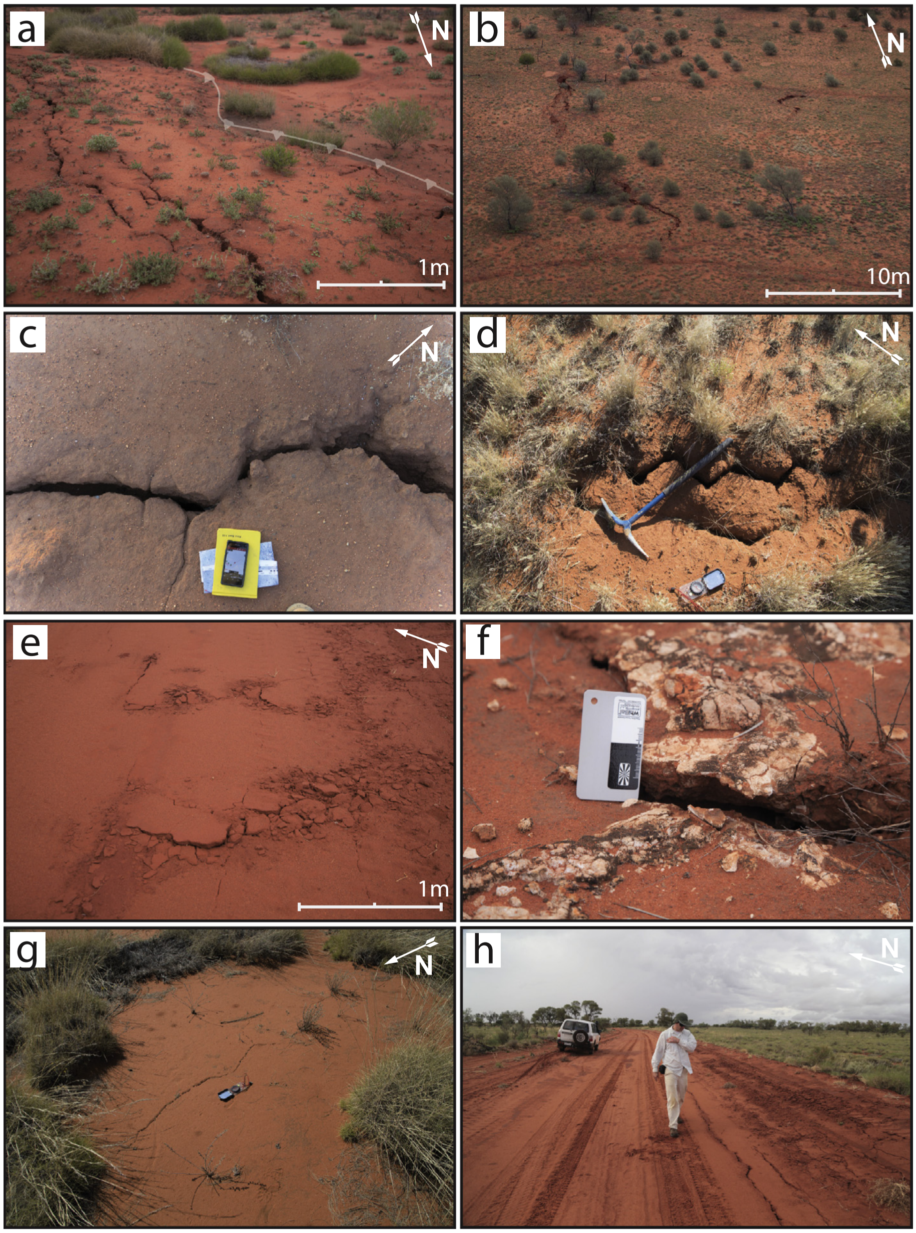

Fig. 5. Observed cracking (a) extensional cracks due to fault-tip folding (b) large extensional cracks/fissures at backward step of scarp (c) transpressional cracking with right lateral movement creating push-up along an extensional fault (d) transtensional cracking with right lateral movement creating slightly offset extensional features (e) compressional pop-ups along access track (f) compressional pop-ups where surface sediment is dominated by calcrete clasts (Fig. 4e) (g) minor cracking observed in 2016, potentially from aftershocks (h) cracking parallel to road (roughly perpendicular to rupture). All photos taken on the hanging-wall.

part to edge collapse) and 25 cm extension at depth (Fig. 5b). Cracks with minimal extension and no observable strike-slip offset were observed across the area including up to 2 km from the scarp on the footwall, and up to 6 km from the scarp on the hanging-wall (Fig. 5g).

Compressional cracks were most commonly observed within a few meters of the surface rupture on the hanging-wall. These cracks were typically less than a metre long with variable strike direction, oblique to the main crack trend (i.e. zig-zag). They were observed where the rupture had only minor vertical offset and particularly where the scarp ran through a slope (e.g. dune edge).

In the month following the event, minor cracks were observed crossing fresh vehicle tracks in the immediate area around aftershocks in the range of M_L 3.0–4.0. During the second field season minor cracking was observed 2 km from the surface rupture on both the footwall and hanging-wall, it cannot be determined if this was related to the main shock, or a result of aftershocks in the region.

2.4. Polygonal cracking

Cracking with a circular or polygonal form was common throughout the observed area up to 5 km from the surface rupture on the hanging-wall, though only a few hundred meters of the footwall. These polygonal cracks occurred around areas of visibly harder and more cemented sand with diameters from 2 to 4 m in inter-dune areas (Fig. 6). These patches of harder sand are generally unvegetated, and commonly termed 'fairy circles' (Walsh et al., 2016). They were most commonly observed to form on flat lying sparsely vegetated grassed areas and within areas of dense spinifex. Active termite and ant nests were occasionally observed within the patches (Fig. 6e, f).

Cracking occurred around all edges of the hard patches of sand (Fig. 6a, b) or along only one edge (Fig. 6c, d). Polygons within a few meters of the surface rupture also experienced cracking through the middle of the polygon. The cracks were generally extensional, but also

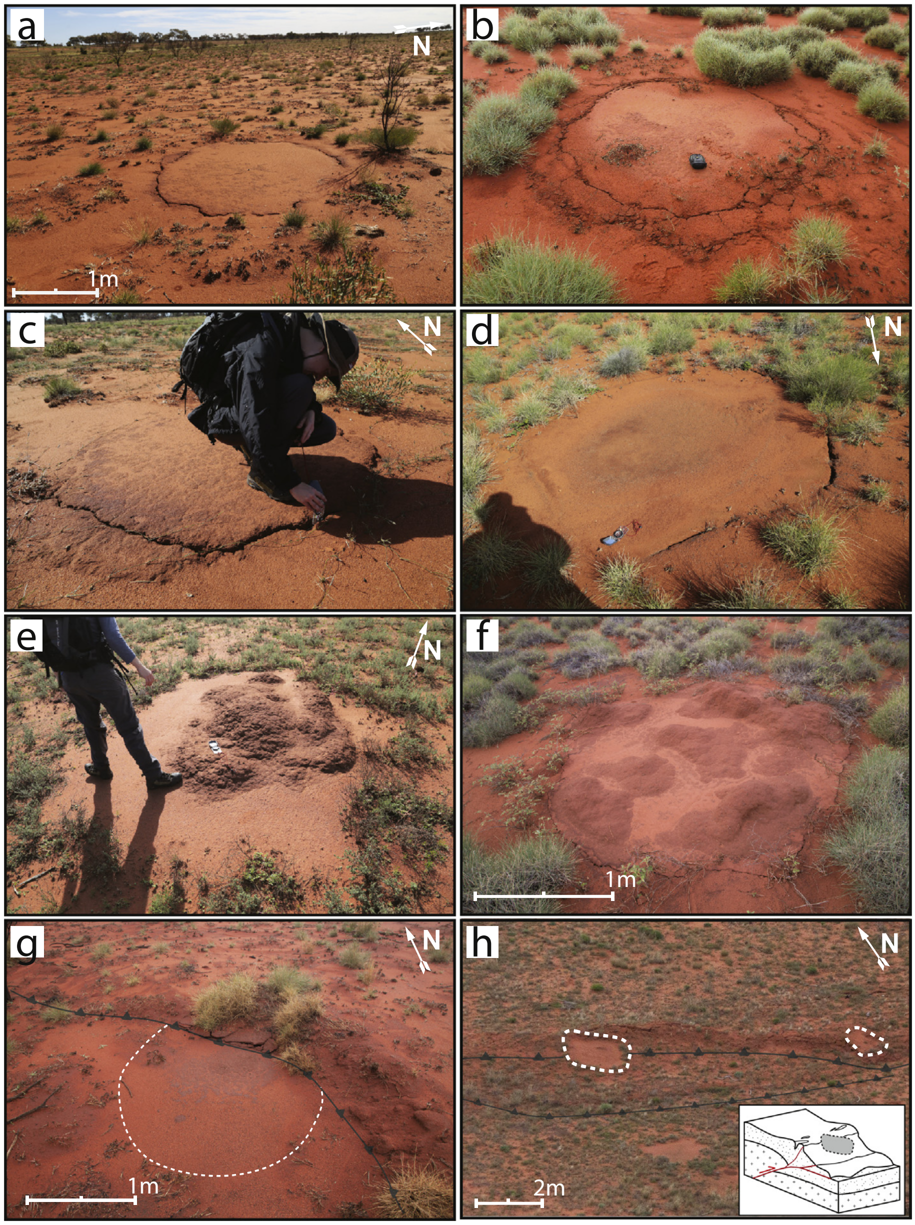

Fig. 6. Polygonal cracking around harder patches of sand (a) cracking around the whole polygon (b) cracking around whole polygon with harder patch now higher than surround sand (c) Cracking around one edge only, with patch now higher than surrounding sand (d) cracking around one edge only with patch now lower than surrounding sand (e) active termite mound on patch with no cracking (f) active ant mound on patch with cracking (g) footwall harder patch thrust over by hanging-wall (h) harder patches 'surfing' duplexing discrete ruptures. All photos (except (g)) taken on the hanging-wall.

showed vertical offset with the hard areas being both above or below the surrounding sand. This vertical offset suggests they acted as rigid pillars within the softer surrounding sand during shaking from the Petermann earthquake, causing the surrounding extensional cracks and vertical settling of the sand around the polygon, or the polygon itself.

Where sand polygons occurred on the footwall along the edge of discretely rupturing scarp, they were observed to be thrust over (Fig. 6g) while on the hanging-wall some polygons had been bent into the rupture itself while experiencing no internal deformation (Fig. 6h).

2.5. Outcrop damage

Several large outcrops of heavily weathered, unfoliated granite up to 20 km from the epicentre experienced rock damage attributed to coseismic strong ground motions (Fig. 7a, b). Shaking affected steeply dipping exfoliation sheets on granite dome edges and boulders/tors. Damaged and fallen rock were found crushing fresh vegetation, with fresh white rock powder at impact sites, and exposed weathering 'shadows' (patches lighter in colour than surrounding patina) indicated dislodged boulders, sheet structures and loose chip movement (Fig. 7c, d). The remains of insects, soil and cobwebs previously inhabiting cracks between rock surfaces were observed on exposed surfaces (Fig. 7b). Damage to larger outcrops was most intense around the edges of outcrops where the outcrop dip is highest.

Where outcrop damage was most severe, rockfalls consisted of sheeting structures (2–15 cm thick), small boulders (40–60 cm diameter), parts of large boulders (20–50 cm thick) and whole large boulders (60–150 cm diameter). Outcrops with minor damage lost near-vertical sheeting structures and had occasional small boulder movement. At the most damaged outcrops rock loss is estimated in the order of 30–50 m^3 decreasing with distance from the surface rupture to < 10 m^3 at outcrops with visible minor damage. Precarious perched

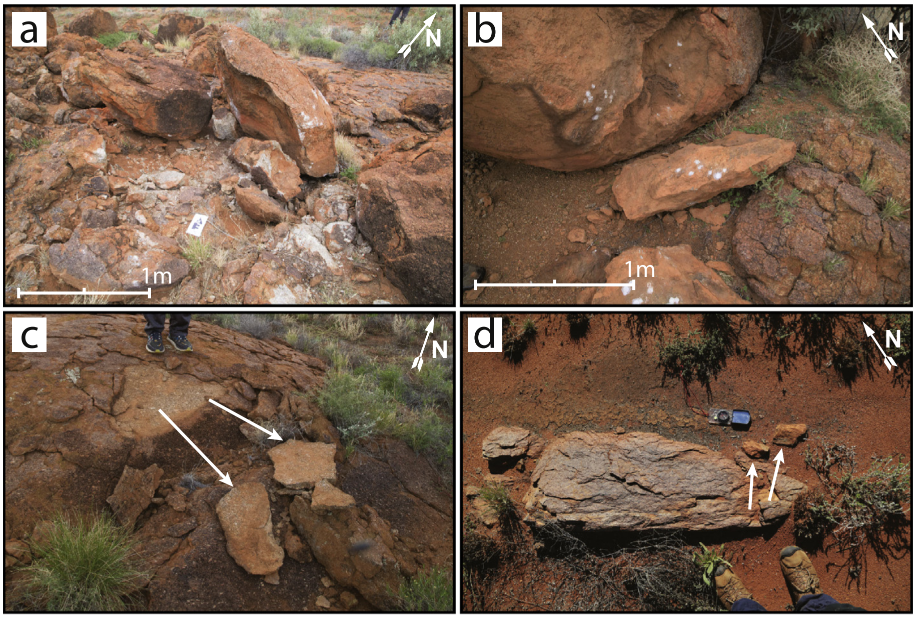

Fig. 7. Outcrop damage (a) boulder fallen off the edge of a 5 m high outcrop onto near-surface bedrock (b) block of outcrop broken along erosion cracks exposing insect nests previously living in the cracks, without which the damage may not have been identified as recent (c) exfoliation chips of low-lying bedrock flipped and displaced due to earthquake (d) displaced flipped chips of small low-lying bedrock outcrop. All photos taken on the hanging-wall.

boulders of varying sizes (20–150 cm diameter) were observed on footwall outcrops 4–50 km from the surface rupture and 20–30 km on the hanging-wall.

Small exfoliation chips of mylonite rock fragments with ~4 cm average thickness were found dislodged and transported from their original locations (Fig. 7c,d). The original location of these chips was clear from damage and fresh dust at detachment sites on the outcrop and chip, exposed weathering 'shadows' on the outcrop and under the surface of chips, and imprinted sand where chips landed on the ground rather than outcrop. The most significant movement included up to 100 cm horizontal distance with < 50 cm vertical distance between the original location and the ground. More commonly the range of movement was 10–40 cm horizontal and < 40 cm vertical distance. The trajectory required for the chips to travel such distances from their original locations suggests a coseismic strong ground motion origin (King et al., 2017).

2.6. Vegetation

Notable damage observed to vegetation and large trees in the near-fault region included tall shrubs fallen down (Fig. 8a), bushes and young trees knocked over/split and killed by surface rupture and subsurface root tear (Fig. 8b,c,d), bark 'exploded' from sides of the tree (Fig. 9a,b), canopies broken off the trunk (Fig. 9c,d), fallen fresh and dead limbs of large desert oaks (Fig. 9e), and a complete trunk split in half (Fig. 9f). These features were observed along the surface rupture, on the hanging-wall within 200 m of the surface rupture, or between step-overs of the scarp. This damage is attributed as coseismic as the intensity and density of damage proximal to the rupture was not observed at distance from the rupture during traverses. Coseismic damage to trees was not consistent in expression along the surface rupture, with many trees, bushes and grasses in the same vicinity as damaged vegetation exhibiting no structural or root damage despite being located on fold structures, cracks, or adjacent to the surface rupture (Fig. 8e, f,g,h). Many burnt-out and dead trunks exist across the region and many of these were observed fallen on both hanging-wall and footwall adjacent to the surface rupture. The age of these fallen and damaged trunks is difficult to determine, they may not be coseismic.

2.7. Holes

Several tens of holes were observed in close proximity or along the surface rupture on the hanging-wall, distinct from deep extensional cracks due to the lack of clear directivity/strike/elongation (images of holes available in supplementary material). Holes were commonly < 1 m diameter and 30 cm depth, with some reaching 3 m diameter and 1 m depth. Holes were most common in inter-dune regions where surface sediment was semi-consolidated and/or clay-rich. No evidence of pre-existing holes is observable in available pre-earthquake satellite imagery of the area. These may represent patches of 'collapsible soils', sandy soils with an open unstable structure where clay, salt or carbonate provide partial bonds between grains which collapse upon saturation and loading. These are found most commonly in aeolian Pleistocene environments (Derbyshire et al., 1995; Rogers, 1995) such as those found in the Petermann area (Hesse, 2010). Seismic stresses have previously been suggested as potential triggers of collapse in unsaturated soils (Rogers, 1995). Dynamic stresses due to Petermann earthquake fault rupture propagation towards the surface may have locally collapsed susceptible surface sediments along the hanging-wall. Further testing of the soil would be required to confirm this theory for hole formation, as opposed to the features relating to collapsed animal burrows or other potential mechanisms.

3. Degradation of observed environmental effects

Field work conducted 16 months after the earthquake found sheetwash, footwall ponding and vegetation growth had significantly obscured and lowered the surface rupture in areas of low vertical offset (Fig. 10a,b,c,d) and obscured much of the surface cracking around the scarp. Many smaller extensional cracks were partially or completely infilled by wind-blown dust and animal movement, however larger cracks were mostly unchanged in the 16 months. Rills had formed across some areas of rupture within a few weeks of the earthquake (Fig. 10e) and minor gullies were locally cutting into the rupture 16 months later (Fig. 10f).

Regional sand availability and transport is thought to be extremely low in upland desert environments such as the Petermann dune system (Hesse, 2010). Based on repeat observations of holes created during the 2012 M_w 5.4 Pukatja earthquake (images available in supplementary information), edge collapse and local sediment sheet wash are likely to infill holes and fissures faster than regional sediment transport, within 10^2 years. We speculate that the largest fissures and holes may infill in 10^3 years. No erosion rate data are known from the granitic landscapes of the Petermann or Mann Ranges. However, cosmogenic radionuclide

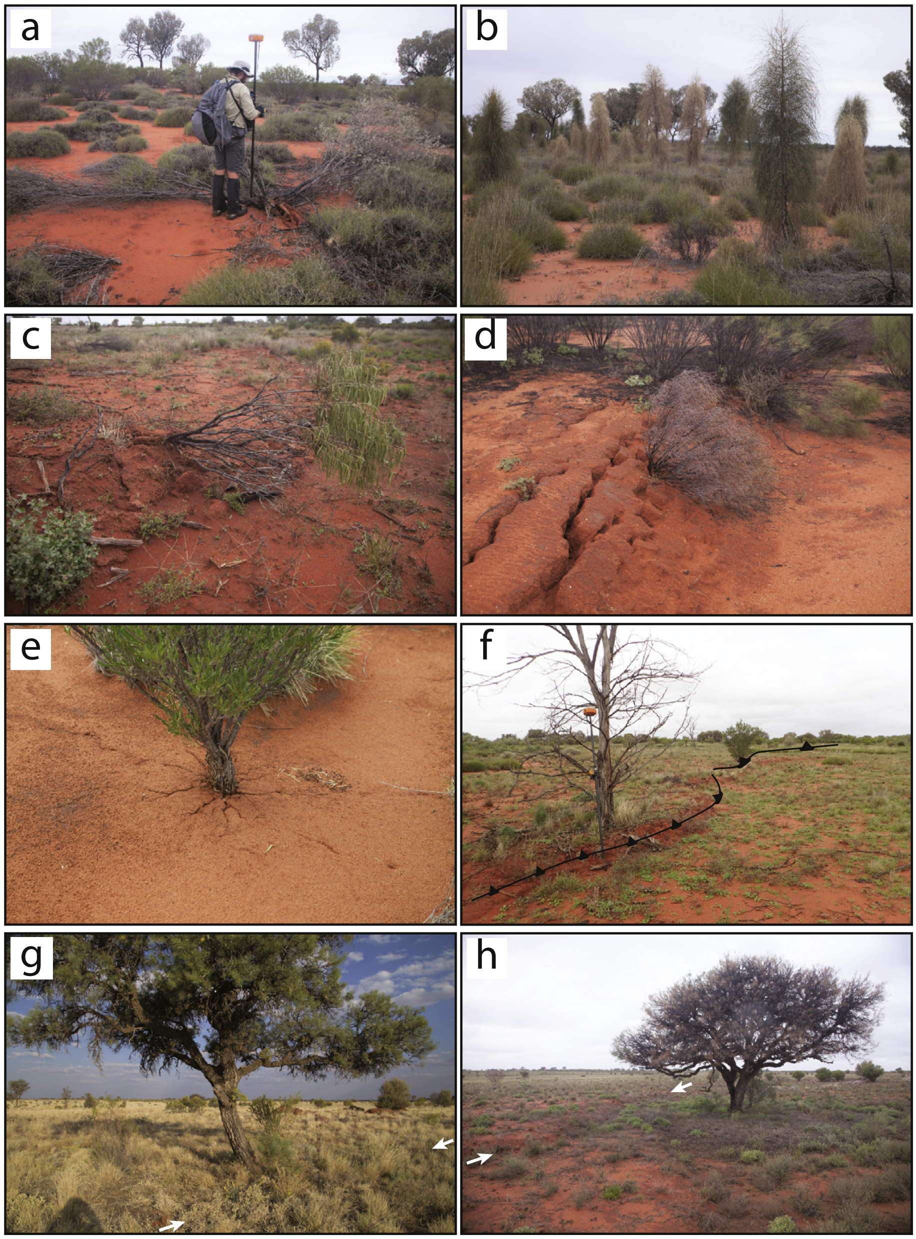

Fig. 8. Minor tree damage (a) small bush collapsed in multiple directions due to strong ground motions (b) grove of immature desert oak trees along the surface rupture with browning leaves due to root-tear (c) and (d) bushes pushed over by hanging-wall rupture tree on hanging-wall rupture (e) cracking around the trunk of a small bush with no damage to the bush (f) and (g) tree on hanging-wall rupture with no damage (h) dying/dead tree on footwall with no other damage, unclear if health of tree is earthquake related.

erosion rates from weathered and sheeting granitic inselbergs from the semi-arid Eyre Peninsula in South Australia provide an acceptable analogue in terms of rock type, outcrop style and climate. Rates of 0.3–0.5 m Ma^{-1} on the top of outcrops, and up to 3.4–5.7 m Ma^{-1} for the lowest platforms of the inselbergs (Bierman and Caffee, 2002) provide a basis to estimate the rate of rock-related EEE degradation in the Petermann Ranges.

Fallen and damaged rocks are now located on sediment or bedrock surfaces and are thus comparatively more susceptible to chemical and physical weathering than in-situ outcrop. Based on erosion rates ranges of 0.3–5.7 Ma^{-1} for near-surface bedrock from Eyre Peninsula inselbergs, these damaged rocks may be completely eroded within 3.5–66 Ka for 2 cm, and 263–5000 Ka for 150 cm thick rocks.

In contrast to the longevity of damaged rock (10^3–10^5 year timescales), evidence for the coseismic nature of the damage such as crushed vegetation, clearly exposed weathering 'shadows', and fresh dust at detachment and impact sites is more transient. This evidence was already difficult to identify a month after the event, and was only visible with careful examination during the second field season.

The density and intensity of displaced chips around the surface rupture may be diagnostic of coseismic damage for a considerable time until they erode away (10^3–10^4 years, based on the above near-surface granitic erosion rate). However, a single displaced chip is not clearly diagnostic of strong ground motion as animals, lightning and vegetation could conceivably displace chips. During the second field season, post-rain ground-covering vegetation obscured many of the displaced chips identified during the first field season.

Vegetation damage was preserved a year after the event, however the coseismic nature of the damage was not as clear. Evidence of lost limbs and bark was obscured by ground cover or weathered by rain, and dead bushes and trees were not clearly recent. We speculate that broken canopies and large fallen limbs might withstand decay and

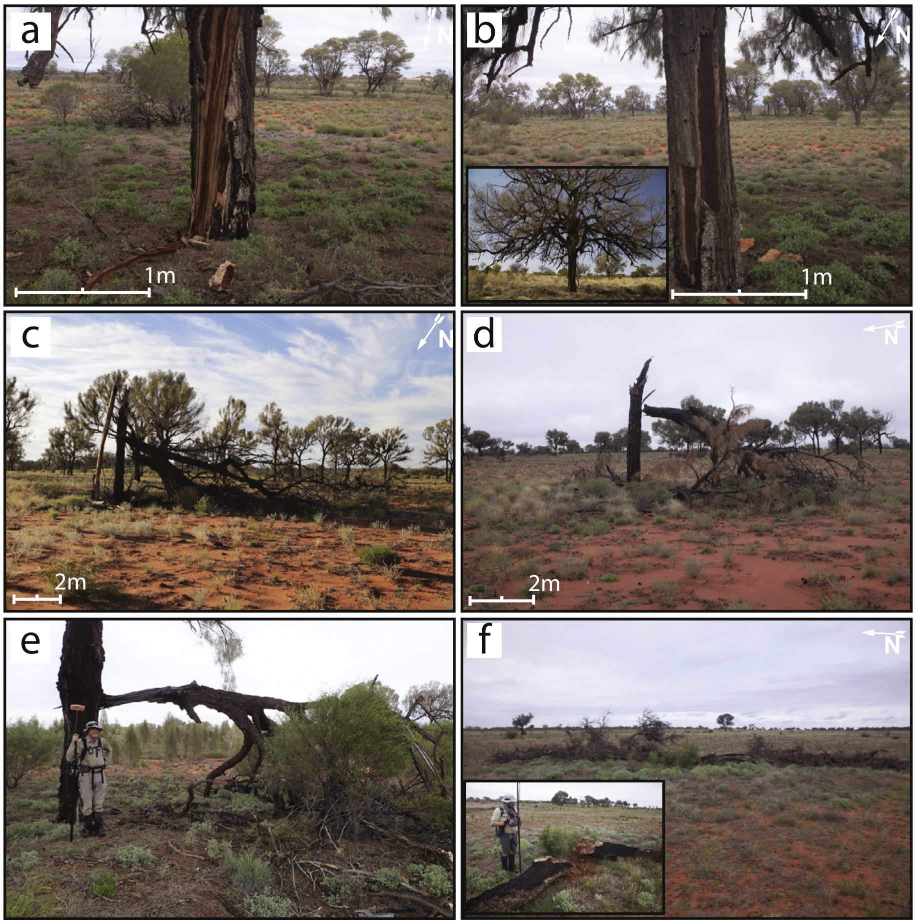

Fig. 9. Major tree damage (a) and (b) bark 'exploded' from tree in wrenching motion near hanging-wall rupture (c) and (d) tree canopies fallen from mature trees (e) large branch fallen from mature tree (f) large tree broken in two along trunk. All images taken on the hanging-wall.

bushfire effects for 10^1–10^2 years. However, attributing them as co-seismic would be extremely difficult after only a few years.

4. Discussion

4.1. Environmental seismic intensity of the Petermann earthquake

EEEs observed during 2016 and 2017 field seasons have been classified using the ESI-07 scale (Table 1 and supplementary material) and mapped in detail (Fig. 11). Isoseismals were manually constructed using visual interpolation between sites where observations were recorded, because automatic fitting using point-density tools created misleadingly dense EEE contour spacing close to the surface rupture. Petermann earthquake surface faulting clearly fits into the description for ESI *X*, at ~20 km length and maximum vertical offset of 0.9 m. This estimate is consistent with Papanikolaou and Melaki (2017), who presented magnitude/ESI relationships for Greek and Mediterranean events with an average ESI of *IX* for magnitude 6.1–6.5 events (n = 14). Serva et al. (2016) report M_w and ESI for events across the world (n = 19), with the events between M_w 5.9–7.1 all classified as ESI *X* (n = 7).

Petermann secondary EEEs are not easily classified using the ESI 2007 scale. ESI *VII* is the only level that provides a clear description of cracking in a desert environment, *"rarely, in dry sand, sand-clay, and clay soil fractures are also seen, up to 1 cm wide"*. This description suggests that extension in dry sand environments is lower, which implies that dry sand cracking at other ESI levels will differ from descriptions for cohesive and saturated soil. We have classified any cracking ≤1 cm as ESI *VII*, cracks > 1 cm as ESI *VIII* and fissures as ESI *X*.

In the absence of direct observations, and with a large number of trees and shrubs affected by seasonal bushfire damage, vegetation damage was difficult to quantify within the ESI scheme. Large desert oaks are common across the area and only a few were observed with obvious earthquake derived damage, leading us to classify this damage as ESI *VIII*. Shrub and small tree damage along the surface rupture was not common or severe, and has been classified as *VI*.

Damage to heavily weathered outcrops of granite in the vicinity of the earthquake, with no significant slope or loose scree, was poorly constrained by ESI descriptions of 'slope movements'. Outcrops with minor damage to weathered vertical sides have been classified as *VI* while outcrops with severe damage have been classified as *VII* based on volume of rock loss and outcrop descriptions.

'Jumping stones' as described in the ESI-07 scale were observed across the field area (Fig. 7) up to 18 km from the surface rupture on the hanging-wall. These displaced rocks fall under ESI *IX* (Serva et al., 2016), significantly increasing the recorded ESI at distance from the surface rupture when compared to the extent of cracking, outcrop damage, polygonal cracking and vegetation damage (Fig. 12).

The ESI-07 scale has been used as a tool to assess epicentral intensity and estimate historic epicentres where EEE descriptions exist in written records (Papathanassiou et al., 2017; Rodríguez-Pascua et al., 2017). Petermann ESI and concentration of EEEs increases with proximity to the surface rupture, rather than towards the epicentre (Fig. 12). ESI isoseismals extend north-east across the epicentral area due to a single crack and displaced rocks observed in the 2017 field season (Fig. 11), which may relate to four M_L 3.2–3.9 aftershocks located 4–8 km from the observed EEEs (Fig. 1b).

Fig. 11 and Fig. 12 highlight ESI increase towards the surface

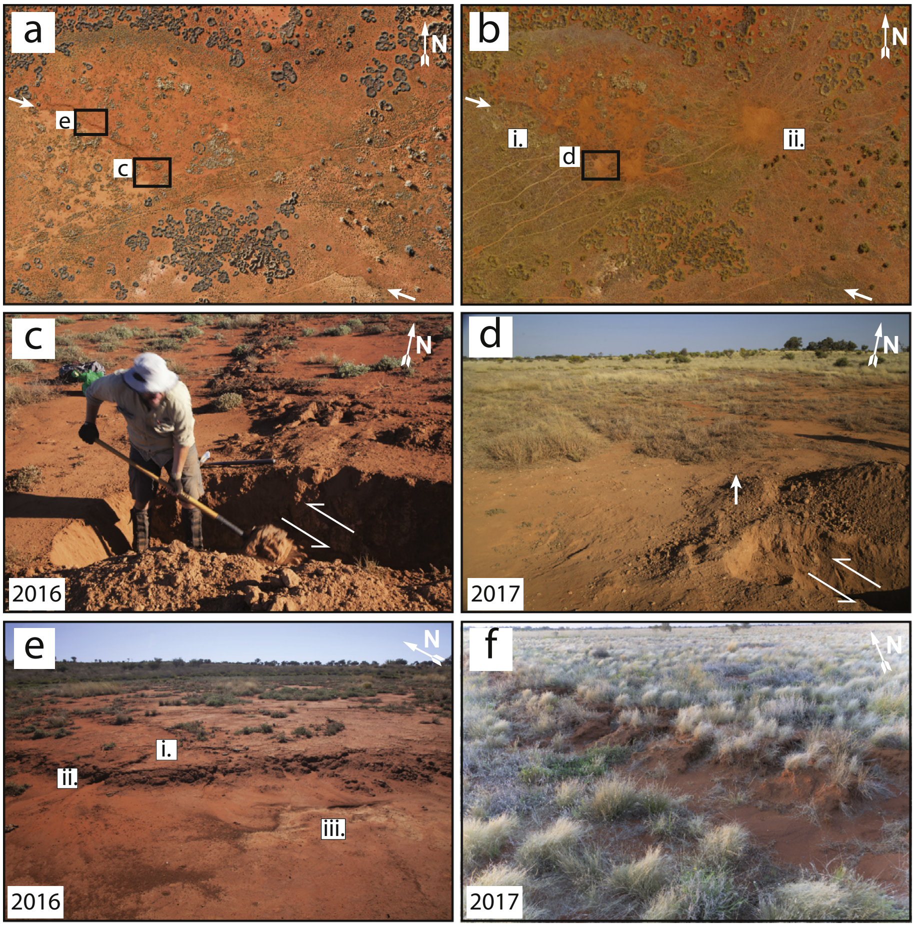

Fig. 10. Denudation and changes along the rupture (a) and (b) comparisons of 2016 and 2017 drone imagery showing i. abundant vegetation growth along the footwall where ponding was observed in 2016, and ii. new camel baths on the hanging-wall (c) and (d) discrete rupture near a hand trench from 2016 (redug in 2017) shows nearly complete denudation of the surface rupture front (e) erosional features along the rupture including i. rills pushing back into the hanging-wall ii. gulling across the hanging-wall and redeposits of sediment on the footwall iii. ponding of water along the rupture on the footwall (f) gully development along the rupture observed 16 months after mainshock after a year of record breaking rainfall events, no observable base-level lowering from sheetwash.

Table 1
Classification of Petermann EEEs into ESI-07 scales, and the total area covered by each ESI level. Classifications based on ESI-07 scale descriptions from Serva et al., 2016.

ESI	Area	Included EEEs[a]
VI	300 km^2	- Small tree/bushes damage - Minor outcrop damage, particularly vertical sides of heavily weathered outcrops
VII	170 km^2	- Cracks ≤1 cm wide - Severe outcrop damage, particularly where not on vertical side of outcrop, or less heavily weathered outcrop.
VIII	138 km^2	- Large tree damage (e.g. canopy collapse) - Cracks >1 cm wide
IX	290 km^2	- Flipped/displaced rock chips
X	12.5 km^2	- Surface rupture, fissures, collapse structures associated with susceptible soils

[a] See Supplementary Material for full classification table based on descriptions in Serva et al., 2016

rupture, particularly on the hanging-wall where strong ground motions and fault rupture propagation combine in the near-surface. This asymmetric distribution has previously been identified where the ESI-07 scale has been applied to the 1999 Chi Chi earthquake (Ota et al., 2009). For strike-slip and high-angle dip-slip faults, ESI-07 isoseismals may define a macroseismic epicentre coincident with an instrumental epicentre. For moderate to shallow dip-slip faults the distance between the epicentre and surface damage (Repi) (Fig. 12c) can be considerably further than the distance between the fault and surface (Rrup), localising damage and macroseismic epicentre closer to the surface rupture/fault tip. In the Petermann event, maximum ESI-07 isoseismials are within uncertainty bounds of instrumental epicentres, but define the surface rupture rather than a macroseismic or instrumental epicentre."

Within the ESI-07 scale an earthquake of ESI *X* should affect an area in the order of 5000 km^2. The distribution of observed EEEs of the Petermann earthquake is an order of magnitude lower, affecting just 300 km^2 (Fig. 11). In the absence of significant topographic or soil-related site effects, the distribution of cracking, outcrop and vegetation damage is limited to the near field region. Jumping stones extend further than other secondary EEEs, particularly on the hanging-wall. These features are thought to be largely controlled by first-motion fault directivity pulses related to fault rupture propagation along a dipping plane (King et al., 2017; Somerville et al., 1997). Almost all other lower ESI data points are covered by the *IX* contour due to the displaced stones, with the area of ESI *IX* significantly larger than that of ESI *VIII* and *VII* (Fig. 11). Our observations suggest the ESI-07 scale may overestimate the true intensity required to displace stones where strong hanging-wall directivity is present. The ESI-07 scale includes many hydrological effects not observable in the arid desert landscape which may have otherwise extended ESI isoseismals out to larger distances.

4.2. ESI-07 scale as a palaeoseismic tool

For the ESI-07 scale to be used for palaeoseismic investigations EEEs must remain identifiable in the landscape on a timescale consistent with the return time of multiple strong ground motion events at a given location. These palaeoseismic time scales are orders of magnitude different depending on the tectonic setting, and the preservation of EEEs is dependent on tectonic setting, local geography, geology and geomorphology. The degradation of Petermann EEEs in an intraplate landscape that has experienced relatively little change during the Holocene offers insight into the potential maximum longevity of EEEs in more dynamic landscapes.

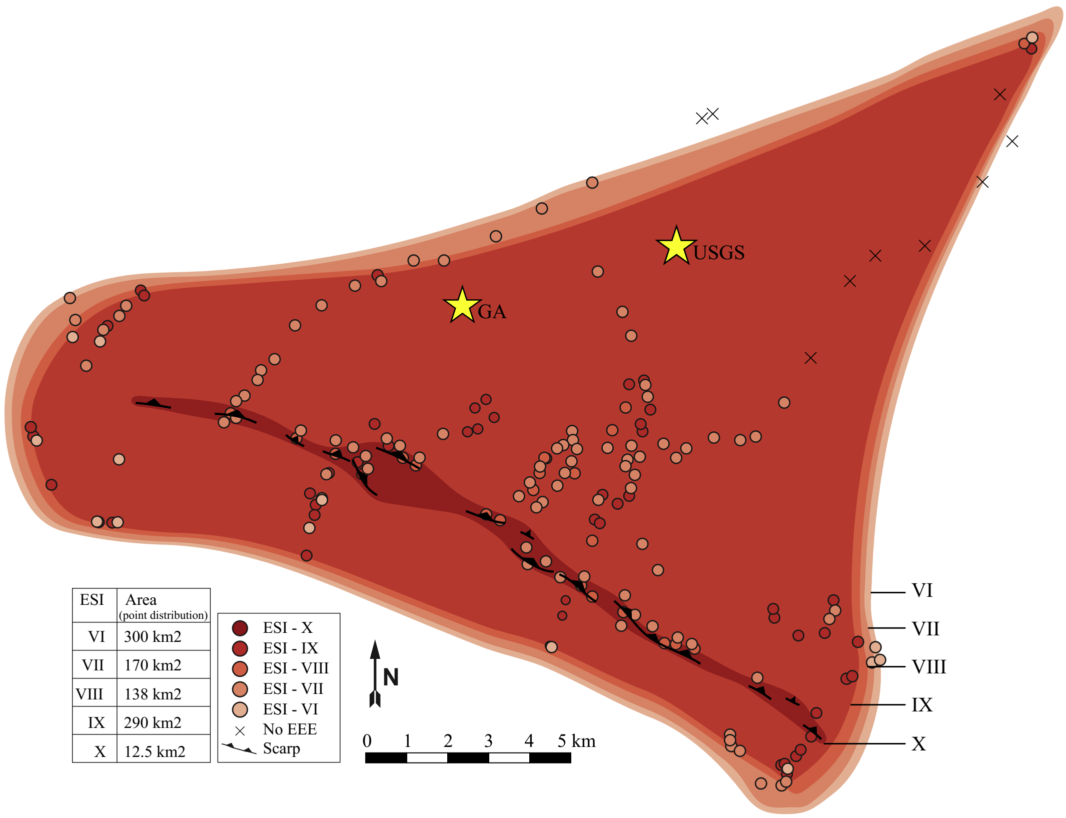

Fig. 11. Environmental Seismic Intensity contour map of observed EEEs. Individual data locations have been combined and data along the surface rupture has been removed to enhance visual clarity, these data are included in Fig. 1. Some relevant data points where no EEEs were observed are included.

Three historic surface ruptures provide comparable geographic examples to assess the longevity of the 2016 Petermann scarp; the 13 km long 1986 M_w 5.8 Marryat Creek (Machette et al., 1993), 32 km long 1988 M_w 6.7 Tennant Creek scarps (Bowman, 1992) and 1.6 km long 2012 M_w 5.4 Pukatja (Ernabella) Scarp (Clark et al., 2014). Levelling data collected four years after the Marryat Creek event (Machette et al., 1993) showed 0.3 m of vertical offset lost from the maximum offset of 0.9 m (the same maximum offset as the Petermann event). Degradation was reported at a similar rate across the Tennant Creek scarp two years after its formation (Clark and McCue, 2003). No repeat survey has occurred along the Pukatja surface rupture to document erosion of the 0.36–0.51 m high scarp (Clark et al., 2014), however part of the scarp with 0.4–0.48 m original offset had lost ~0.1–0.2 m vertical height as observed in 2016 during a brief visit by the authors. In contrast, a section of the 37 km long 1968 Meckering earthquake scarp that was fenced off as a geological monument has persisted as a topographic high for 50 years in part thanks to the ferricrete horizon defining the scarp (Clark and McCue, 2003).

Many secondary EEEs observed in the Petermann earthquake have a high chance of remaining in the landscape for 1000–100,000 years (Fig. 13a). At the current rate of geomorphic change in the area, rockfalls, large displaced rocks and large (> 1 m extension) cracking are likely to persist for 10^3–10^5 years. Given the slow growth rates of desert oak trees, recorded as being in excess of 1000 years old (*Parks Australia, 2018*), trees with lost limbs and canopies may retain evidence for seismic events for decades to hundreds of years.

Despite the potential longevity of EEEs in the landscape, damage may not be identifiable and attributable to a seismic origin on the same timescale, limiting EEE usefulness for palaeoseismic investigations (Fig. 13b). Nine days after the event, authors observed rock fall damage to a hanging-wall outcrop close to the surface rupture, with large boulders fallen from the edges of the outcrop onto the bedrock surface below. The authors found the same rock fall difficult to identify 23 days after the earthquake due to heavy rainfall removing much of the fresh rock dust and the uneven colouring of the old exposed surfaces making the fresh colouring difficult to identify. As noted, vegetation growth 16 months after the earthquake had obscured many of the displaced chips previously identified. Aeolian processes and small animal movement (insects, marsupials) was observed actively obscuring minor extensional cracks during the 2017 field season. Holes and large extensional cracks are expected to persist for 10^2–10^3 years. However, they are prone to ponding and edge collapse which may obscure them in the landscape on a much shorter timescale.

Petermann scarp sections underlain by near-surface bedrock may persist as topographic highs far longer than those with thick sections of sandy top-soil. However, these sections constitute at most a quarter of the total scarp length and are not continuous, casting doubt as to whether the relatively low offset would be recognised as earthquake related topography in the future. Previous attempts to identify neotectonic fault scarps on a continental scale were limited by the available data sources (Clark et al., 2012). For example linear features < 2–3 m are not readily discoverable on 1–3 arc sec SRTM data (Clark, 2010; Clark et al., 2011). It is questionable whether a continental-scale investigation would identify the relatively short and low Petermann scarp at current height, or after 10^3–10^5 years (the potential recurrence for Australian faults) (Clark et al., 2012) without prior knowledge of the rupture location.

Observations across two field seasons suggest that the ability to identify EEEs and confidently attribute them to a seismic origin (Fig. 13b) is in most instances orders of magnitude lower than the estimated preservation time of each EEE (Fig. 13a). Fig. 14 illustrates how the Petermann ESI field map (Fig. 11) may change with time when comparing the projected degradation rates of EEEs (Fig. 13a) with the projected decrease in confidently attributable EEEs (Fig. 13b). The most significant differences between the expected preservation of EEE and observable EEE maps are attributable to rock falls and displaced rocks.

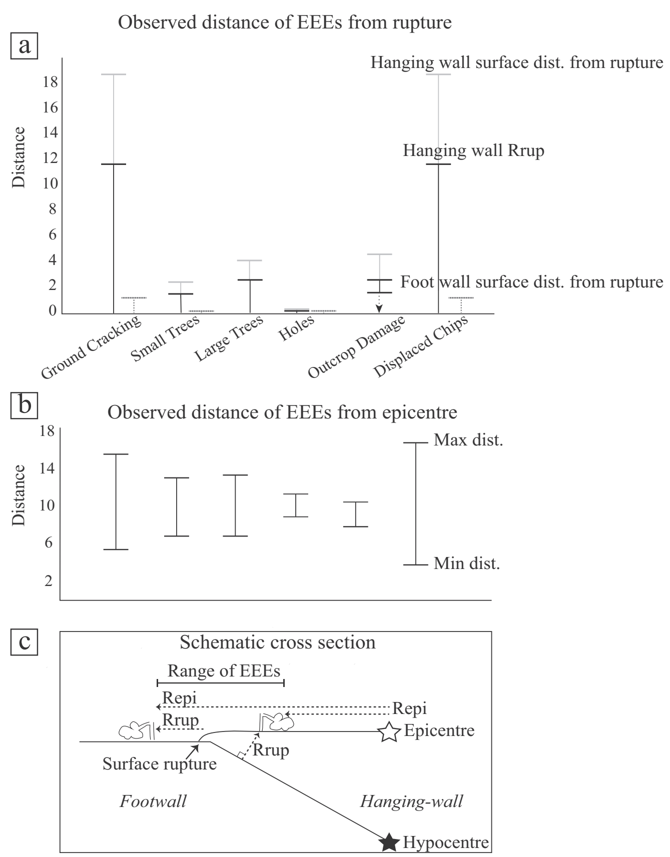

Fig. 12. (a) The observed maximum distance from the surface rupture for each category of EEE with footwall observations as dashed line, true hanging-wall Rrup distance in black, and hanging-wall ground distance from the surface rupture in grey. Some EEEs were not observed on the footwall. Outcrop damage is limited by the lack of large outcrops near the rupture but is projected to extend to the surface rupture. (b) The observed maximum and minimum distances from the USGS instrumental epicentre for each category of EEE (c) schematic diagram demonstrating the difference in distance between Rrup and Repi for an observed EEE on the footwall and hanging-wall (dip not to scale, refer to Fig. 1 for available fault dip data for Petermann event).

Erosion rates are low enough that rocks will still be in place 1000 years post-event, but are very difficult to identify as earthquake related on much shorter timescales. Similarly, the surface rupture may still be discoverable on high resolution DEMs after 50 years, but given the erodibility of soft sediments, may not be visible in the field in that same timeframe.

We propose that most EEEs will not be identifiable and confidently attributable to a seismic origin within 10–1000 years, despite an estimated preservation of 1000–100,000 years. As shown in Fig. 14, after just 50 years the area of observable environmental damage will be in the order of 10^2 km^2, while after 1000 years observable EEEs may only cover 45 km^2. The inability to identify EEEs over short timescales makes the ESI-07 scale difficult to apply in Australia where recurrence rates of $M_w > 6.5$ earthquakes exceed those ranges, and distances make detailed mapping difficult. The difficulties identified in assigning EEEs to the Petermann earthquake event, in a region characterised by very low rates of geomorphic change, suggests that applying the ESI-07 scale to palaeoseismic events in regions with high geomorphic change would be extremely challenging.

The limited temporal preservation and spatial extent of EEEs following the Petermann earthquake demonstrate the difficulties in using the ESI-07 scale for palaeoseismic mapping in Australia. However, there are still regions where the ESI-07 scale could be useful to investigate palaeoseismic activity. Large intraplate earthquakes appear to have extended aftershock sequences over hundreds of years (Stein and Liu, 2009) which may explain Australian seismic hot spots in the Simpson Desert (NT/SA) and west of Lake Mackay (WA). Rigorous and careful field mapping may identify patterns in density and intensity of EEEs that could be used to test this hypothesis.

Careful and thorough mapping could also be applied to neotectonic scarps across the country (Clark et al., 2011, 2012) to establish a minimum age constraint (i.e. limit of EEE degradation) on the most recent large event, provide an estimate of magnitude, and define the true rupture extent of degraded scarps.

As demonstrated on Fig. 1, the Australian continent contains regions where: the spatial density of historical earthquakes and neotectonic structures are relatively high (e.g., Flinders Ranges; (Quigley et al., 2010, 2006)); where historic seismicity is relatively low but where abundant neotectonic structures have been identified (e.g., eastern Nullarbor Plain; (Hillis et al., 2008)); areas where seismicity is relatively high but where neotectonic structures are only sparsely recognised (e.g., northwestern Australia; (Clark et al., 2011)); and areas where both seismicity and neotectonic structure densities are low (SE

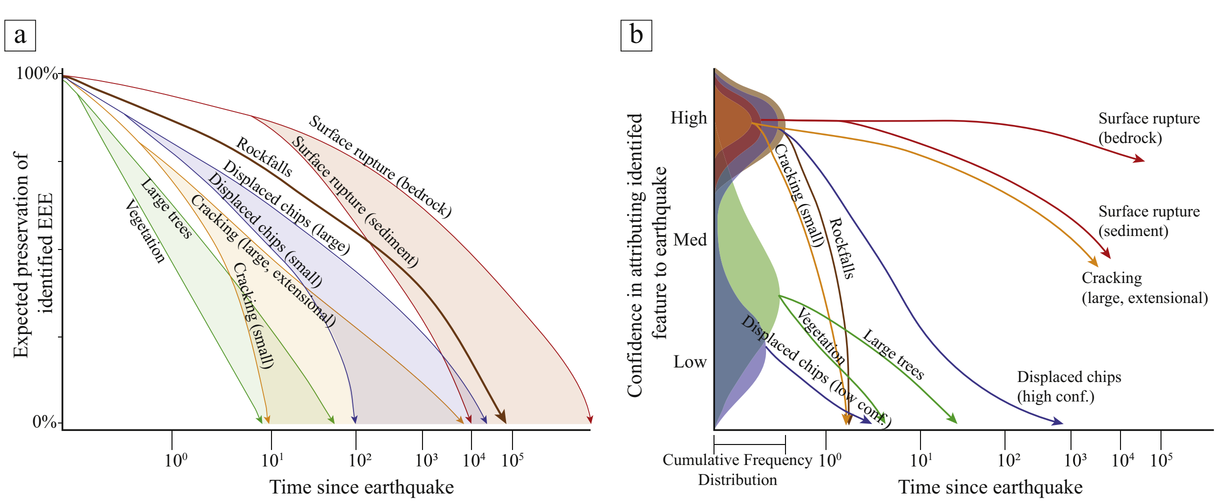

Fig. 13. Conceptual charts showing the preservation and observability of EEEs through time (a) graph showing the expected preservation of EEEs through time for the Petermann earthquake based on estimates of EEE degradation as detailed in Sections 3 and 4.2 (b) graph showing the level of confidence in attributing immediately observed damage to the earthquake (High, Med, Low) based on field observations detailed in Section 3, and how that confidence changes through time.

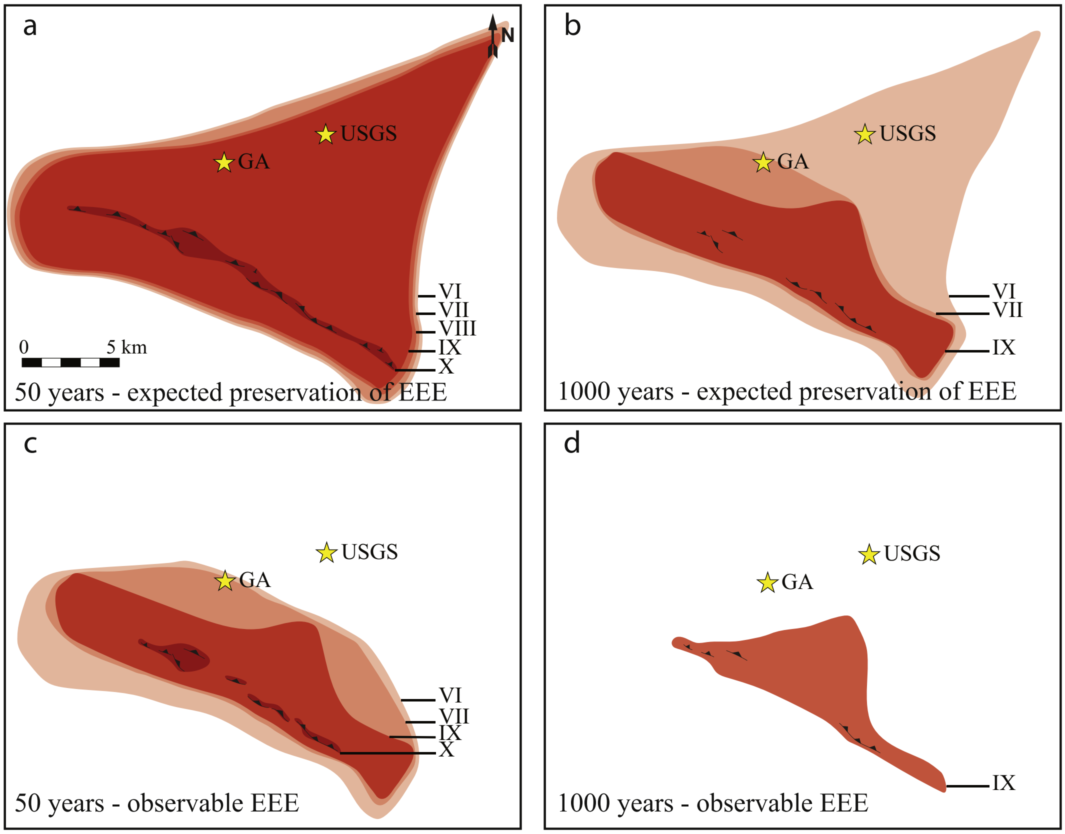

Fig. 14. Expected change to the ESI contour map at 50 and 1000 years post event based on (a) and (b) the expected preservation of EEEs based upon the persistence of features in the landscape (i.e. Fig. 13a) and (c) and (d) the potential to identify and confidently attributing EEEs to a seismic origin (i.e. Fig. 13b) as discussed in the text.

Queensland; (Clark et al., 2011)). Some areas of high seismicity and neotectonic feature density are associated with uplifted, fault-bounded topography, and faults with hundreds of meters of Plio-Quaternary displacement. This suggests persistent strain localisation into intraplate zones of mechanically and/or thermally weakened lithosphere over geological (i.e. > 5–10 Myr) time-scales (Balfour et al., 2015; Hillis et al., 2008; Holford et al., 2011; Quigley et al., 2010), consistent with models for focused intraplate strain proposed elsewhere (Grollimund and Zoback, 2001; Kenner and Segall, 2000; Liu and Stein, 2016; Sykes, 1978; Zhan et al., 2016).

In areas where seismicity rates and neotectonic structure densities do not correlate and where no geomorphic evidence for long-term localisation of intraplate strain is present, it is likely that seismicity is spatiotemporally episodic and migratory over historical-to-geological timescales (Clark, 2010; Leonard and Clark, 2011; Liu et al., 2011; Pilia et al., 2013). Earthquake environmental effects provide potential opportunities to evaluate end-member models of intraplate seismicity such as persistent strain localisation (e.g., Sandiford and Egholm, 2008) vs. migratory behaviour (e.g., Calais et al., 2016) and hypotheses pertaining to the duration of continental aftershock sequences (e.g., Stein and Liu, 2009). For example, the presence of prehistoric EEEs such as displaced rock fragments in areas of historical seismicity might provide geological evidence for preceding strong earthquakes and persistent seismicity extending over prehistoric to historic timescales.

Akin to paleo-liquefaction studies (e.g. Tuttle, 2002), EEEs are one of the best available tools to gain a deeper understanding of intraplate earthquake characteristics. This is particularly the case in arid Australia, where the short historical record of seismicity demands utility of the geologic record to better characterise earthquake hazard, low population density minimizes human disturbance of prehistoric EEEs, and where slow erosion and climatic aridity favour preservation of prehistoric EEEs. The ESI-07 scale is the only applicable macroseismic intensity scale for many remote historic surface ruptures, and the only scale with possible use in describing pre-European Holocene earthquakes. However, the application of the scale is complicated by factors described in this study, including the limited areal extent of damage, short observational timeframe of many EEEs, and logistical difficulties in conducting fine-scale field work in remote regions. In practice, high potential uncertainties in the values and intensities of ESI isoseismal maps suggest the ESI-07 scale constitutes but one of a series of paleoseismic approaches that might be utilized in seismic hazard analyses.

5. Conclusion

Thousands of individual EEEs were identified following the 20th May 2016 Petermann earthquake, classified into five main types (rupture, cracking, outcrop, displaced chips, vegetation) and assigned Environmental Seismic Intensity values. The lack of topographic, geological, geomorphic and anthropological complexity provides a rare opportunity to investigate the distribution of EEEs without significant site response effects. We were able to observe how fault geometry affects EEE intensity and distribution and characterise the preservation potential of EEEs without anthropogenic interference.

Petermann EEEs are spatially clustered around the surface rupture and not the epicentral region. Similar asymmetric ESI distributions have been previously described for reverse faulting events (Ota et al., 2009) and attributable to hanging-wall/footwall effects and fault-rupture propagation.

Repeat field seasons to observe the Petermann EEEs offer insight into the projected preservation of EEEs through time and their applicability to palaeoseismic investigations. Based on degradation of damage following significant rainfall events, and applying available erosion rates estimates, EEEs will persist from 10's of years (vegetation, minor cracking) to thousands (displaced chips, large cracks) and potentially 10^4–10^6 years (rock falls, surface rupture). However, our observations also show that the ability to observe EEEs and confidently ascribe them to a uniquely seismic origin decreases significantly faster, within just 10^0–10^3 years. ESI estimations will therefore underestimate the true magnitude and intensity of the event with time.

The difficulties in observing and confidently attributing EEEs to a seismic origin decreases the applicability of the ESI-07 scale in Australian palaeoseismic investigations where recurrence intervals can be 10^3–10^5 years on an individual fault (Clark et al., 2012). Low potential for associating EEEs with earthquake events in Australia, where rates of geomorphic change are very low, suggests the geological proxies used to construct ESI-07 scale isoseismals in this study may have limited applicability to palaeoseismic studies in areas with higher rates of geomorphic change.

This event provides the first Australian test of the ESI-07 scale, with a catalogue of thousands of individual EEEs across five distinct categories. The ESI intensity (*X*) of the earthquake (M_w 6.1) is in line with the intensity attributed to other moderate magnitude earthquakes (Papanikolaou and Melaki, 2017; Serva et al., 2016) though the area of observed secondary EEEs is an order of magnitude smaller than the ESI-07 scale suggests for ESI *X*. The Petermann earthquake provides a new event for inclusion in future attenuation relationships and the observed effects may help to improve the applicability of the ESI-07 scale across different landscapes and tectonic regimes.

Acknowledgements

We thank the Australian Research Council for providing funding for this project through Discovery Grant #DP170103350, and the Australian Government Research Training Program Scholarship for providing Tamarah's scholarship. We thank Fabian Prideaux, Craig Bugden and Ayers Rock Automotive for their invaluable field support at short notice in surprisingly bad weather. We also thank Gary Gibson and Abe Jones for their field support and aftershock data analysis. GG-Cat is maintained by Gary Gibson, University of Melbourne and can be accessed by contacting the authors. We would like to acknowledge the Pitjantjatjara people (Aṉangu) as the traditional owners of the land on which our field work took place. We thank Alessandro Michetti and an anonymous reviewer for comments that improved this manuscript. T. King received a Baragwanath Travel Scholarship from the University of Melbourne which supported part of this field work. D. Clark publishes with the permission of the Chief Executive Officer of Geoscience Australia.

Appendix A. Supplementary data

Supplementary data to this article can be found online at https://doi.org/10.1016/j.tecto.2018.10.010.

References

Ali, Z., Qaisar, M., Mahmood, T., Shah, M.A., Iqbal, T., Serva, L., Michetti, A.M., Burton, P.W., 2009. The Muzaffarabad, Pakistan, earthquake of 8 October 2005: surface faulting, environmental effects and macroseismic intensity. Geol. Soc. Lond. Spec. Publ. 316, 155–172. https://doi.org/10.1144/SP316.9.

Allen, T., Leonard, M., Collins, C., 2012. The 2012 Australian seismic hazard map – catalogue and ground motion prediction equations. In: Australian Earthquake Engineering Society 2011 Conference, 18–20 Nov., Barossa Valley, South Australia, pp. 18–20.

Parks Australia, 2018. Fact Sheet: Uluru-Kata Tjuta National Park. (accessed 16th October 2018). http://www.environment.gov.au/system/files/resources/49b7c8d1-19cf-4eaf-bb4b-19df844ead07/files/uktnp-a4factsheet-flora-small.pdf.

Balfour, N.J., Cummins, P.R., Pilia, S., Love, D., 2015. Localization of intraplate deformation through fluid-assisted faulting in the lower-crust: the Flinders Ranges, South Australia. Tectonophysics 655, 97–106. https://doi.org/10.1016/j.tecto.2015.05.014.

Bell, J.G., Kilgour, P.L., English, P.M., Woodgate, M.F., Lewis, S.J., Wischusen, J.D.H., 2012. WASANT Palaeovalley Map - Distribution of Palaeovalleys in Arid and Semi-arid WA-SA-NT.

Bierman, P.R., Caffee, M., 2002. Cosmogenic exposure and erosion history of Australian bedrock landforms. Bull. Geol. Soc. Am. 114, 787–803. https://doi.org/10.1130/0016-7606(2002)114<0787:CEAEHO>2.0.CO;2.

Blumetti, A.M., Grützner, C., Guerrieri, L., Livio, F., 2017. Quaternary earthquakes: Geology and palaeoseismology for seismic hazard assessment. Quat. Int. 451, 1–10. https://doi.org/10.1016/j.quaint.2017.04.002.

Bowman, J.R., 1992. The 1988 Tennant Creek, northern territory, earthquakes: a synthesis. Aust. J. Earth Sci. 39, 651–669. https://doi.org/10.1080/08120099208728056.

Calais, E., Camelbeeck, T., Stein, S., Liu, M., Craig, T.J., 2016. A new paradigm for large earthquakes in stable continental plate interiors. Geophys. Res. Lett. 43, 10,621–10,637. https://doi.org/10.1002/2016GL070815.

Chen, X.Y., Bowler, J.M., Magee, J.W., 1993. Late Cenozoic stratigraphy and hydrologic history of lake Amadeus, a central Australian playa. Aust. J. Earth Sci. 40, 1–14. https://doi.org/10.1080/08120099308728059.

Clark, D., 2010. Identification of quaternary scarps in southwest and central west Western Australia using dem-based hill shading: Application to seismic hazard assessment and neotectonics. Int. J. Remote Sens. 31, 6297–6325. https://doi-org.ezp.lib.unimelb.edu.au/10.1080/01431161003631592.

Clark, D., McCue, K., 2003. Australian paleoseismology: towards a better basis for seismic hazard estimation. Ann. Geophys. 46, 1087–1106. http://hdl.handle.net/2122/1005.

Clark, D., Dentith, M., Wyrwoll, K.-H., Yanchou, L., Dent, V., Featherstone, W., 2008. The Hyden fault scarp, Western Australia: paleoseismic evidence for repeated quaternary displacement in an intracratonic setting. Aust. J. Earth Sci. 55, 379–395. https://doi.org/10.1080/08120090701769498.

Clark, D., McPherson, A., Collins, C.D.N., 2011. Australia's Seismogenic Neotectonic Record aCase for Heterogeneous Intraplate Deformation. Geoscience Australia Record.

Clark, D., McPherson, A., Van Dissen, R.J., 2012. Long-term behaviour of Australian stable continental region (SCR) faults. Tectonophysics 566–567, 1–30. https://doi.org/10.1016/j.tecto.2012.07.004.

Clark, D., McPherson, A., Allen, T.I., De Kool, M., 2014. Coseismic surface deformation caused by the 23 March 2012 Mw 5.4 Ernabella (Pukatja) earthquake, central Australia: implications for fault scaling relations in cratonic settings. Bull. Seismol. Soc. Am. 104, 24–39. https://doi.org/10.1785/0120120361.

Crone, A.J., De Martini, P.M., Machette, M.N., Okumura, K., Prescott, J.R., 2003. Paleoseismicity of two historically quiescent faults in Australia: implications for fault behavior in stable continental regions. Bull. Seismol. Soc. Am. 93, 1913–1934. https://doi.org/10.1785/0120000094.

Derbyshire, E., Dijkstra, T., Smalley, I.J., 1995. Genesis and Properties of Collapsible Soils. Springer, Loughborough, UK.

Edgoose, C.J., Scrimgeour, I.R., Close, D.F., 2004. Geology of the Musgrave Block, Northern Territory. Northern Territory Geological Survey.

Gordon, F.R., Lewis, J.D., 1980. The Meckering and Calingiri earthquakes October 1968 and March 1970. Geological Survey of Western Australia Bulletin. .

Grollimund, B.R., Zoback, M.D., 2001. Did deglaciation triger intraplate seismicity in the New Madrid seismic zone? Geology 29, 175. https://doi.org/10.1130/0091-7613(2001)029<0175:DDTISI>2.0.CO;2.

Guerrieri, L., Tatevossian, R., Vittori, E., Comerci, V., Esposito, E., Michetti, A.M., Porfido, S., Serva, L., 2007. Earthquake environmental effects (EEE) and intensity assessment: the INQUA scale project. Boll. Soc. Geol. Ital. 126, 375–386.

Hesse, P.P., 2010. The Australian desert dunefields: formation and evolution in an old, flat, dry continent. Geol. Soc. Lond. Spec. Publ. 346, 141–164. https://doi.org/10.1144/SP346.9.

Hillis, R.R., Sandiford, M., Reynolds, S.D., Quigley, M.C., 2008. Present-day stresses, seismicity and neogene-to-recent tectonics of Australia's "passive" margins: intraplate deformation controlled by plate boundary forces. Geol. Soc. Lond. Spec. Publ. 306, 71–90. https://doi.org/10.1144/SP306.3.

Holdgate, G.R., Wallace, M.W., Gallagher, S.J., Smith, A.J., Keene, J.B., Moore, D., Shafik, S., 2003. Plio-Pleistocene tectonics and eustacy in the Gippsland Basin, southeast Australia: evidence from magnetic imagery and marine geological data. Aust. J. Earth Sci. 50, 403–426. https://doi.org/10.1046/j.1440-0952.2003.01004.x.

Holdgate, G.R., Wallace, M.W., Gallagher, S.J., Wagstaff, B.E., Moore, D., 2008. No mountains to snow on: Major post-Eocene uplift of the East Victoria Highlands; evidence from Cenozoic deposits. Aust. J. Earth Sci. 55, 211–234. https://doi.org/10.1080/08120090701689373.

Holford, S.P., Hillis, R.R., Hand, M., Sandiford, M., 2011. Thermal weakening localizes intraplate deformation along the southern Australian continental margin. Earth Planet. Sci. Lett. 305, 207–214. https://doi.org/10.1016/j.epsl.2011.02.056.

Kenner, S.J., Segall, P., 2000. A mechanical model for intraplate earthquakes: application to the New Madric Seismic Zone. Science 80 (289). https://doi.org/10.1126/science.289.5488.2329.

King, T.R., Quigley, M.C., Sandiford, M., 2017. Near-source strong ground motions inferred from displaced geologic objects. In: Australian Earthquake Engineering Society 2017 Conference. ACT, Canberra.

Leonard, M., 2008. One hundred years of earthquake recording in Australia. Bull. Seismol. Soc. Am. 98, 1458–1470. https://doi.org/10.1785/0120050193.

Leonard, M., Clark, D., 2011. A record of stable continental region earthquakes from Western Australia spanning the late Pleistocene: Insights for contemporary seismicity. Earth Planet. Sci. Lett. 309, 207–212. https://doi.org/10.1016/j.epsl.2011.06.035.

Liu, M., Stein, S., 2016. Mid-continental earthquakes: spatiotemporal occurrences, causes, and hazards. Earth Sci. Rev. 162, 364–386. https://doi.org/10.1016/j.earscirev.2016.09.016.

Liu, M., Stein, S., Wang, H., 2011. 2000 years of migrating earthquakes in North China: how earthquakes in midcontinents differ from those at plate boundaries. Lithosphere 3, 128–132. https://doi.org/10.1130/L129.1.

Machette, M., Crone, A., Bowman, R.J., 1993. Geologic Investigations of the 1986 Marryat Creek, Australia, Earthquake: Implications for Paleoseismicity in Stable Continental Regions. USGS Bulletin.

Mcpherson, A., Clark, D., Macphail, M., Cupper, M., 2014. Episodic post-rift deformation in the south-eastern Australian passive margin: evidence from the lapstone structural complex. Earth Surf. Process. Landf. 39, 1449–1466. https://doi.org/10.1002/esp.3535.

Michetti, A.M., Esposito, E., Guerrieri, L., Porfido, S., Serva, L., Tatevossian, R., Vittori, E., Audemard, F., Azuma, T., Clague, J., Comerci, V., Gurpinar, A., McCalpin, J., Mohammadioun, B., Morner, N.A., Ota, Y., Roghozhin, E., 2007. Intensity scale ESI 2007. Mem. Descr. della Cart. Geol. D'Italia 74.

Ota, Y., Azuma, T., Lin, Y.N., 2009. Application of INQUA Environmental Seismic Intensity Scale to recent earthquakes in Japan and Taiwan. Geol. Soc. Spec. Publ. 316, 55–71. https://doi.org/10.1144/SP316.4.

Papanikolaou, I., Melaki, M., 2017. The Environmental Seismic Intensity Scale (ESI 2007) in Greece, addition of new events and its relationship with magnitude in Greece and the Mediterranean; preliminary attenuation relationships. Quat. Int. 451, 37–55. https://doi.org/10.1016/j.quaint.2017.05.044.

Papanikolaou, I.D., Papanikolaou, D.I., Lekkas, E.L., 2009. Advances and limitations of the Environmental Seismic Intensity scale (ESI 2007) regarding near-field and far-field effects from recent earthquakes in Greece: implications for the seismic hazard assessment. Geol. Soc. Lond. Spec. Publ. 316, 11–30. https://doi.org/10.1144/SP316.2.

Papathanassiou, G., Valkaniotis, S., Ganas, A., 2017. Evaluation of the macroseismic intensities triggered by the January/February 2014 Cephalonia, (Greece) earthquakes based on ESI-07 scale and their comparison to 1867 historical event. Quat. Int. 451, 234–247. https://doi.org/10.1016/j.quaint.2016.09.039.

Pilia, S., Rawlinson, N., Direen, N.G., Cummins, P.R., Balfour, N., 2013. Structural controls on localized intraplate deformation and seismicity in Southern Australia: insights from local earthquake tomography of the Flinders Ranges. J. Geophys. Res. Solid Earth 118, 2176–2190. https://doi.org/10.1002/jgrb.50168.

Quigley, M.C., Cupper, M., Sandiford, M., 2006. Quaternary faults of south-central Australia: palaeoseismicity, slip rates and origin. Aust. J. Earth Sci. 53, 285–301. https://doi.org/10.1080/08120090500499271.

Quigley, M.C., Sandiford, M., Cupper, M., 2007a. Distinguishing tectonic from climatic controls on range-front sedimentation. Basin Res. 19, 491–505. https://doi.org/10.1111/j.1365-2117.2007.00336.x.

Quigley, M.C., Sandiford, M., Fifield, L.K., Alimanovic, A., 2007b. Landscape responses to intraplate tectonism: quantitative constraints from 10Be nuclide abundances. Earth Planet. Sci. Lett. 261, 120–133. https://doi.org/10.1016/j.epsl.2007.06.020.

Quigley, M.C., Clark, D., Sandiford, M., 2010. Tectonic geomorphology of Australia. Geol. Soc. Lond. Spec. Publ. 346, 243–265. https://doi.org/10.1144/SP346.13.

Quigley, M.C., Hughes, M.W., Bradley, B.A., van Ballegooy, S., Reid, C., Morgenroth, J., Horton, T., Duffy, B., Pettinga, J.R., 2016. The 2010–2011 Canterbury earthquake sequence: environmental effects, seismic triggering thresholds and geologic legacy. Tectonophysics 672–673, 228–274. https://doi.org/10.1016/j.tecto.2016.01.044.

Rajabi, M., Tingay, M., Heidbach, O., Hillis, R., Reynolds, S.D., 2017. The present-day stress field of Australia. Earth Sci. Rev. 168, 165–189. https://doi.org/10.1016/j.earscirev.2017.04.003.

Robinson, A.C., Copely, P.B., Canty, P.D., Baker, L.M., Nesbitt, B.J., 2003. A Biological Survey of the Anangu Pitjantjatjara Lands, South Australia 1991–2001. South Aust. Dep. Environ, Heritage, Adelaide.

Rodríguez-Pascua, M.A., Pérez-López, R., Garduño-Monroy, V.H., Perucha, M.A., Israde-Alcántara, I., 2017. Estimation of the epicentral area of the 1912 Acambay earthquake (M 6.9, Mexico) determined from the earthquake archaeological effects (EAE) and the ESI07 macroseismic scale. Quat. Int. 451, 74–86. https://doi.org/10.1016/j.quaint.2017.06.045.

Rogers, C.D.F., 1995. Types and distribution of collapsible soils. In: Derbyshire, E., Dijkstra, T., Smalley, I.J. (Eds.), Genesis and Properties of Collapsible Soils. Springer, Loughborough, UK, pp. 1–17.

Sanchez, J.J., Maldonado, R.F., 2016. Application of the ESI 2007 scale to two large earthquakes: South Island, New Zealand (2010 Mw 7.1), and Tohoku, Japan (2011 Mw 9.0). Bull. Seismol. Soc. Am. 106, 1151–1161. https://doi.org/10.1785/0120150188.

Sandiford, M., Egholm, D.L., 2008. Enhanced intraplate seismicity along continental margins: some causes and consequences. Tectonophysics 457, 197–208. https://doi.org/10.1016/j.tecto.2008.06.004.

Serva, L., Vittori, E., Comerci, V., Esposito, E., Guerrieri, L., Michetti, A.M., Mohammadioun, B., Mohammadioun, G.C., Porfido, S., Tatevossian, R.E., 2016. Earthquake hazard and the Environmental Seismic Intensity (ESI) scale. Pure Appl. Geophys. 173, 1479–1515. https://doi.org/10.1007/s00024-015-1177-8.

Silva, P.G., Reicherter, K., Grützner, C., Bardají, T., Lario, J., Goy, J.L., Zazo, C., Becker-Heidmann, P., 2009. Surface and subsurface palaeoseismic records at the ancient Roman city of Baelo Claudia and the Bolonia Bay area, Cádiz (south Spain). Geol. Soc. Lond. Spec. Publ. 316, 93–121. https://doi.org/10.1144/SP316.6.

Somerville, P., Smith, N.F., Graves, R.W., Abrahamson, N.A., 1997. Modification of empirical strong ground motion attenuation relations to include the amplitude and duration effects of rupture directivity. Seismol. Res. Lett. 68, 199–222. https://doi.org/10.1785/gssrl.68.1.199.

Stein, S., Liu, M., 2009. Long aftershock sequences within continents and implications for earthquake hazard assessment. Nature 462, 87–89. https://doi.org/10.1038/nature08502.

Sykes, L.R., 1978. Intraplate seismicity, reactivation of preexisting zones of weakness, alkaline magmatism, and other tectonism postdating continental fragmentation. Rev. Geophys. 16, 621–688. https://doi.org/10.1029/RG016i004p00621.

Tuttle, M.P., 2002. The earthquake potential of the New Madrid Seismic Zone. Bull. Seismol. Soc. Am. 92, 2080–2089. https://doi.org/10.1785/0120010227.

Wallace, M.W., Dickinson, J.A., Moore, D.H., Sandiford, M., 2005. Late Neogene strandlines of southern Victoria: a unique record of eustasy and tectonics in southeast Australia. Aust. J. Earth Sci. 52, 279–297. https://doi.org/10.1080/08120090500139455.

Walsh, F.J., Sparrow, A.D., Kendrick, P., Schofield, J., 2016. Fairy circles or ghosts of termitaria? Pavement termites as alternative causes of circular patterns in vegetation of desert Australia. Proc. Natl. Acad. Sci. 113, 201607860. https://doi.org/10.1073/pnas.1607860113.

Zhan, Y., Hou, G., Kusky, T., Gregg, P.M., 2016. Stress development in heterogenetic lithosphere: insights into earthquake processes in the New Madrid Seismic Zone. Tectonophysics 671, 56–62. https://doi.org/10.1016/j.tecto.2016.01.016.